SUPPLEMENTAL MATERIAL

Myocardial Rev-erb-mediated diurnal metabolic rhythm and obesity paradox

Shiyang Song, MD[1,2 #], Chih-Liang Tien, PhD[3 #], Hao Cui, MD, PhD[4 #], Paul Basil, PhD[1,5], Ningxia Zhu, PhD[1], Yingyun Gong, PhD[1], Wenbo Li, PhD [1], Hui Li, MS[3], Qiying Fan, PhD[6], Jong Min Choi, PhD[7], Weijia Luo, PhD[8], Yanfeng Xue, PhD[1], Rui Cao, PhD[1], Wenjun Zhou, PhD[1], Andrea R. Ortiz, BS[7], Brittany Stork, BS[7], Vatsala Mundra, BS[1], Nagireddy Putluri, PhD[7], Brian York, PhD[7], Maoping Chu, MD, PhD[2], Jiang Chang, MD, PhD[8], Sung Yun Jung, PhD[7], Liang Xie, PhD[6], Jiangping Song, MD, PhD[4] *, Lilei Zhang, MD, PhD[3] *, Zheng Sun, PhD[1,6] *

[1] Department of Medicine, Division of Diabetes, Endocrinology and Metabolism, Baylor College of Medicine, Houston, Texas, USA
[2] Children's Heart Center, Institute of Cardiovascular Development and Translational Medicine, The Second Affiliated Hospital and Yuying Children's Hospital of Wenzhou Medical University, Wenzhou, China
[3] Department of Molecular and Human Genetics, Baylor College of Medicine, Houston, Texas, USA
[4] State Key Laboratory of Cardiovascular Disease, Fuwai Hospital; National Center for Cardiovascular Diseases, Chinese Academy of Medical Sciences (CAMS) and Peking Union Medical College (PUMC), Beijing, China
[5] Department of Critical Care, Division of Anesthesiology, Critical Care and Pain Medicine, University of Texas MD Anderson Cancer Center, 1515 Holcombe Blvd, Unit 110, Houston, TX, 77030-4009, USA
[6] Department of Medicine, Division of Atherosclerosis and Vascular Medicine, Cardiovascular Research Institute (CVRI), Houston, Texas, USA
[7] Department of Molecular and Cellular Biology, Baylor College of Medicine, Houston, Texas, USA
[8] Center for Genomic and Precision Medicine, Texas A&M University, Institute of Biosciences and Technology, Houston, Texas, USA

[#] Equal contributions
* Correspondence:
fwsongjiangping@126.com, lilei.zhang@bcm.edu, zheng.sun@bcm.edu

Index

Expanded Methods

Mice

Rev-erbα^{loxP} (Nr1d1$^{tm1.2Rev}$, MGI ID 5426700), Rev-erbβ^{loxP} (Nr1d2$^{tm1.1Rev}$, MGI ID 5426699), αMHC-Cre (RRID:IMSR_JAX:011038), and αMHC-MerCreMer (RRID:IMSR_JAX:005657) mouse lines were previously described[19–22]. All mice were on the C57BL/6 genetic background. Male and female mice at the age of 2-8 months were used for experiments unless indicated otherwise in figure legends or the main text. We used both male and female mice for the initial echocardiography analysis and did not observe obvious sex differences. We then used male mice for omics studies for easy comparisons among different conditions and datasets, considering the high cost of these experiments. We then validated the transcriptomic results in female mice using RT-qPCR analyses. We performed HFHSD dietary rescue experiments in both male and female mice and found similar results. All mice were group-housed (3-4 mice per cage) in a 12 h light/ 12 h dark (7 am - 7 pm) facility with free access to a chow diet. For MCM mice, tamoxifen at 75mg/kg was i.p. injected daily for 5 consecutive days. Mice locomotor activity and energy expenditure were measured with the Comprehensive Lab Animal Monitoring System for Home Cages (CLAMS-HC) and the Oxymax software (Columbus Instruments). Mice were acclimated to the monitoring environments for at least 48 hours before the experiment. The mice were continuously monitored for 130 hours under the normal light-dark cycles while mice were freely allowed to access food and water. Oxygen consumption was normalized to lean tissue mass. Etomoxir was dissolved in DMSO at 10 ug/ul for stock and was diluted with saline immediately before i.p injection at 20 mg/kg bodyweight. 2-Deoxy-D-glucose (2-DG) was diluted in saline at 50 ug/ul for stock and was i.p. injected at 500 mg/kg bodyweight. To increase dietary sugars, we supplemented drinking water with 20% glucose, 20% sucrose, or 20% fructose, respectively. Water was made fresh and replaced every 2 days. All the animal procedures followed the guidelines of the Institutional Animal Care and Use Committee (IACUC) at Baylor College of Medicine.

Echocardiography

The Vevo 2100 VisualSonics ultrasound system (Visual Sonics Inc.) was used with an attached Integrated Rail System III for imaging acquisition. Mice were anesthetized with 2% isoflurane mixed with 100% oxygen through an inhalation tube. The core body temperature of the mouse was monitored by a rectal temperature probe and maintained at around 37°C by a tensor lamp throughout the procedure, and the heart rate was maintained at 400-500 bpm. Two-dimensional images were obtained at 2.5-3 frames/s using a 15 MHz probe (RMV 707B, Visual Sonics) in the parasternal short-axis views to guide M-mode analysis at the midventricular level. Image measurement and analysis were performed by researchers who were blinded to the mouse genotype.

Histology

Hearts were fixed in 4% paraformaldehyde in PBS overnight at 4 °C and incubated in 30% sucrose in PBS at 4 °C overnight, followed by embedding in paraffin and section at 6 μm thickness. Trichrome staining was performed at the neuropathology core following the standard protocol. For immunofluorescence staining, heart sections were permeabilized with permeabilization solution (0.1% TritonX-100, 0.1% sodium citrate) followed by antigen retrieval, blocking, and incubation with primary antibodies (anti-WGA, Fisher scientific, cat # W11261; anti-Cardiac troponin T: ABclonal, cat # A4914). For WGA staining, quantification analysis of relative cross-section area was processed by ImageJ software. For cardiac troponin T staining, slides were incubated in the fluorescence-conjugated secondary antibody (Invitrogen, cat # A-11035), and then TUNEL assay (Roche, cat # 11684795910) was performed following the manufacturer's instructions.

Western blot and RT-qPCR

Hearts were lysed in a modified RIPA buffer containing 2% SDS and supplemented with phosphatase and protease inhibitors. Lysates were resolved by Tris-glycine SDS-PAGE, transferred to PVDF membrane, and blotted with antibodies against Rev-erbα (Cell Signaling Technology, cat # 13418), GAPDH (Cell Signaling Technology, cat # 2118L), Bmal1 (Cell Signaling Technology, cat # 14020S), Ran (ABclonal, cat # A0976), OXPHOS proteins (MitoSciences, cat # MS604), Gpam (ABclonal, cat # A6610), Ppara (ABclonal, cat # A6697), Ucp3 (ABclonal, cat # A16996), Acss1 (ABclonal, cat # A15007), Acadm (ABclonal, cat # A4567), CD36 (ABclonal, cat # A19016), Acadl (ABclonal, cat # A1266), Ech1 (ABclonal, cat # A12944), Hadhb (ABclonal, cat # A5716), Hsp90 (Cell Signaling Technology, cat # 4874). Images were acquired using LumiQuant AC600 (Acuronbio Technology Inc), quantification analysis was processed by ImageJ software. Total RNA was extracted using TRIzol (Sigma) and RNeasy Mini Kit (Qiagen). Reverse transcription and quantitative PCR were performed with the High-Capacity RT kit, SYBR Green PCR Master Mix, and the Quant Studio 6 instrument (Life

Science) using the relative quantification method with standard curves. 18S RNA was used as the housekeeping denominator.

Isolation and culture of adult mouse cardiomyocytes

Adult mouse cardiomyocytes were obtained from freshly harvested adult hearts at 2 months of age at night using the Langendorff method[23]. Mice were treated with heparin (5 IU/g body weight) via intraperitoneal injection 30 minutes before anesthetization with 3% isoflurane through an inhalation tube. The heart was rapidly excised, and the aorta was cannulated onto a Langendorff apparatus and perfused with 8 ml perfusion buffer, followed by 50 ml of recirculating Liberase Blendzyme type 1 (Roche) digestion buffer. The heart tissue was removed, shredded, and filtered through 100μm sterile cell strainers. The supernatant was collected, and then CaCl2 was added in a graded fashion to sequentially increase the Ca2+ concentration to 500 μM[24]. The suspension was then seeded on laminin-coated culture dishes overnight at 37°C in a 5% CO2 incubator. The media was replaced on the second day to wash away unattached cells. siRNAs (Horizon, Cat # M-051721-01, Cat # M-059128-01, and Cat # M-063246-01) were used to knock down Rev-erbα, Rev-erbβ, and E4bp4, respectively, in adult cardiomyocytes. DharmaFECT 1 Transfection Reagent (Horizon, Cat # T-2001-02) was used for siRNA transfection following the manufacture's instruction.

Cell culture, siRNA transfection, and recombinant DNA

The AC16 human cardiomyocyte cell line was cultured in DMEM/F12 (Sigma Cat # D6434) containing 12.5% fetal bovine serum (FBS) and 1% antibiotics (streptomycin and penicillin). Cells were incubated at 37℃ at 5% CO2. Experiments were performed when the cell population reached around 70% confluence. All experiments were repeated at least three times. siRNAs (Horizon, Cat # M-003411-02-0005, Cat # M-003432-00-0005, and Cat # L-012704-00-0005) were used to knock down Rev-erbα, Rev-erbβ, and E4bp4, respectively, in AC16 cells. DharmaFECT 1 Transfection Reagent (Horizon, Cat # T-2001-02) was used for siRNA transfection following the manufacture's instruction. For overexpressing E4bp4, the pcDNA3.1-E4bp4 plasmid (Addgene 34572)[25] was cotransfected with a GFP plasmid using the jetPRIME transfection reagent (Polyplus, Cat # 114-07), with the GFP plasmid alone serving as the negative control. GFP-positive cells were sorted and collected at 50h after transfection, followed by RT-qPCR and isotope tracer studies.

Radioactive isotope tracing

For fatty acids oxidation, adult mouse cardiomyocytes or AC16 cells were incubated in the culture medium supplemented with BSA-conjugated [9,10-^{3}H(N)]-palmitate and carnitine for 2 h at 37 °C in the incubator. The resultant $^{3}H_2O$ in the incubation solution was separated from precursors using ion-exchange columns (DOWEX 1X4-400) and was measured by a scintillation counter[26]. For glucose oxidation, adult mouse cardiomyocytes were incubated in the culture medium supplemented with D-[^{14}C(U)]-Glucose for 2.5 h at 37 °C in the incubator. The resultant $^{14}CO_2$ was collected using the filter paper containing 400 ul 5N NaOH and then measured by a scintillation counter [27]. For cardiomyocytes glucose uptake, 2-[^{3}H(N)]-deoxy-D-glucose was used in the presence or absence of 20 μM cytochalasin B, an inhibitor of glucose transport. The cardiomyocytes were washed three times with PBS before lysis. Intracellular glucose was determined by subtracting the ^{3}H counting values in the presence of cytochalasin B from that without cytochalasin B[26]. Cells from one mouse were treated as one biological replicate.

Mitochondrial DNA, respiratory enzyme activity, and cellular respirometry

For mitochondrial DNA copy number analysis, heart samples were lysed in lysis buffer (67mM Tris, 16.6mM Ammonium Sulfate, 6.5 mM MgCl2, 1% 2-Me, 0.5% Triton X-100, 1mg/ml Proteinase K) to extract total DNA. qPCR was performed to quantify mtND1 (GTGGCTCATCTACTCCACTGA, TCGAGCGATCCATAACAATAA), a mitochondrial gene, after normalized to a nuclear gene Ndufv1. SDH enzyme activity was measured by the succinate dehydrogenase activity colorimetric assay kit (Sigma, Cat # MAK197) following the manufacturers' instructions. The oxygen consumption rate was determined using a Seahorse Bioscience XF24 Extracellular Flux Analyzer with a mitochondrial stress test kit. AC16 cells were cultured on XF24 microplates in DMEM/F12 with 12.5% FBS. The culture medium was switched to starvation medium (0.1 g/L glucose, 1% FBS) at 24h before the assay. Cellular respiration was then assayed in the presence of BSA-conjugated palmitate, first at the baseline, then after serial addition of mitochondrial inhibitor oligomycin (1 μmol/L), mitochondrial uncoupler carbonyl cyanide p-trifluoromethoxyphenylhydrazone (FCCP, 1 μmol/L), and respiratory chain inhibitor antimycin A and rotenone (1 μmol/L each). ATP turnover is calculated by subtracting oligomycin-dependent respiration

from baseline respiration. Respiratory capacity was calculated by subtracting antimycin A-dependent respiration from the FCCP-dependent respiration following the manufacture's instruction.

RNA-seq and data processing

RNA-seq was performed using total RNA extracted from left ventricles in mice at 2 months of age (n = 3 at each condition, total of 36 samples). RNA was isolated using Trizol reagent (Sigma) followed by RNeasy Mini Kit (Qiagen). The KO vs. WT samples were sequenced on the BGI MGISEQ-2000 platform with PE100 and 6 Gb total clean reads per sample. The sequencing data was filtered with SOAPnuke (v1.5.2) by removing reads containing sequencing adapter, reads whose low-quality base ratio (base quality less than or equal to 5) is more than 20%, and reads whose unknown base ('N' base) ratio is more than 5%. The resultant clean reads were obtained and stored in FASTQ format and mapped to the reference genome GRCm38.p6 using HISAT2 (v2.0.4). Bowtie2 (v2.2.5) was applied to align the clean reads to the reference coding gene set, and the expression level of genes was calculated with RSEM (v1.2.12). The differential expression analysis was performed using the DESeq2 (v1.4.5). GO and KEGG enrichment analysis of annotated different expressed genes was performed by DAVID Bioinformatics Resources 6.7. The z-score was calculated using the formula $z = (x-\mu)/\sigma$, where x is the FPKM value for each individual sample, μ is the population mean for all WT and KO samples at all ZTs (36 samples total), and σ is the population standard deviation of all 36 samples. Analyzed RNA-seq results of Bmal1-CKO vs. WT hearts[28] was downloaded from GSE43073.

ChIP-seq and data processing

Mouse hearts were harvested at ZT9 and ZT21 (6 male WT mice at 2.5 months old at each time point). After nuclei isolation, PCM-1 antibodies (Sigma, cat #HPA023370) were used to purify cardiomyocyte nuclei. Two heart samples were combined in one tube for sonication on the Covaris S220 sonicator. Sonication conditions were as follows: peak power 140, Duty factor 8, cycles/burst 200, 18 min. ChIP was performed with the Rev-erbα antibody (Cell signaling, cat # 13418). The precipitated DNA was then pooled and amplified according to the guideline of Illumina, followed by sequencing on illumine nextseq 500. Sequenced reads were aligned to the reference mouse genome (mm10) using Bowtie 2 (version 2.3.4.2). Non-redundant and uniquely mapped reads were extended to 100 bp in both 5' and 3' directions and used for downstream analysis. Read coverage for every 10 bp bins was calculated using the deepTools bamCoverage (version 3.3.0) function, avoiding blacklist regions of the mouse genome (ENCODE project). Genome browser tracks were visualized in Integrative Genome Browser (IGV version 1.5). Peak calling was performed on unique reads with MACS2 (2.1.2) using input as control. Peaks with $q < 0.05$ and 4-fold over input were used for heat map and Venn diagram comparisons between ZT9 and ZT21. Common and differential peaks at ZT9 and ZT21 were defined by at least one basepair overlap between peaks using the intersect function of BEDTools v2.26.0. For heat map, deepTools computeMatrix and plotHeatmap (version 3.3.0) were used to summarize coverage scores over Rev-erbα peaks. The color key indicates the minimum and maximum frequency of the ChIP signal. Stringent peaks with $p < 1 \times 10^{-5}$ and ≥ 1 read per million mapped reads that were only detected at ZT9 (but not at ZT21) were used for motif analyses. Peaks within 10 kb of the transcription start sites (TSSs) of DEGs were used for further analysis. Motif analyses were performed using sequences within +/- 100 bp of the center of the peaks with HOMER function findMotifsGenome.pl, on default parameters. Bmal1 ChIP-seq data[29] were downloaded from GSE110602 and random non-DEGs were generated using random sampling function, R Project version 4.0.5.

Proteomics

For proteomics profiling, 3 male mice at each genotype (WT and Rev-CKO) were harvested at each time-point of the 3 ZTs (ZT6, 14, and 22) at 2.5 months old. Dissected mouse heart tissues were pulverized and added with 10 sample volumes of lysis buffer (50mM Ammonium Bicarbonate, 1mM $CaCl_2$). Tissue suspensions were snap-frozen using liquid nitrogen, thawed at 37°C, and boiled at 95°C for 3 min to lyse tissue. All freeze-thaw-denaturation procedures were repeated three times. Lysates were double digested with 1/20 and 1/100 of trypsin (GenDepot, T9600) overnight and 4h at 37°C, respectively. Double-digested peptides were fractionated with micro pipet tip C18 column into 15 fractions and pooled into 5 fractions as described previously[30]. Fractionated peptides were subjected to nanoLC-MS/MS analysis with nanoLC-1200 (Thermo Scientific) coupled to Orbitrap Fusion Lumos mass spectrometer (Thermo Scientific) with NSI source. The peptides were loaded onto an in-house Reprosil-Pur Basic C18 (1.9 μm, Dr. Maisch GmbH, Germany) trap column (2 cm length, 100 μm i.d.) and separated by 5 cm column (150um i.d.) with a 75 min discontinuous gradient of 4-24 % of acetonitrile/0.1% formic acid at a flow rate of 800 nl/min. Separated peptides were directly electro-sprayed into the mass spectrometer. Precursor MS spectrum was scanned at 300-1400 m/z 120k resolution at 400 m/z, $5x10^5$ AGC

target (50 ms maximum injection time) by Orbitrap. Then, the top 50 strongest ions were scanned by Quadrupole with 2 m/z isolation window, 15 s exclusion time (±7 ppm), fragmented by HCD with 32 normalized collision energy, and detected by Ion trap with rapid scan range, $5x10^3$ AGC target, and 35 ms of maximum injection time. Obtained MS/MS spectra were searched against the target-decoy Mouse RefSeq database (release 2020) in Proteome Discoverer 2.1 interface (PD 2.1, Thermo Fisher) with the Mascot algorithm (Mascot 2.4, Matrix Science). Dynamic modifications of the acetylation of the N-terminus and oxidation of methionine were allowed. The precursor mass tolerance was confined within 20 ppm with fragment mass tolerance of 0.5 daltons and a maximum of two missed cleavages was allowed. Assigned peptides were filtered with 1% false discovery rate (FDR) using percolator validation based on q-value. Label-free proteomics data were assigned to gene ID and calculated with the iBAQ algorithm for abundance by GPgrouper[31]. Differentially expressed proteins between two groups were determined by t-test. GO analyses were performed using DAVID or iPathwayGuide as mentioned in the figure legends. The z-score was calculated using the formula $z = (x-\mu)/\sigma$, where x is the quantification value for each individual sample, μ is the population mean for all samples, and σ is the population standard deviation of all samples.

Lipidomics

Heart ventricle tissues were harvested from male mice at 3 months old (n = 3 at each condition) and were snap-frozen in liquid nitrogen. Lipids were extracted as previously described [32–34]. Lipids were separated on a Shimadzu CTO-20A Nexera X2 UHPLC systems, 1.8 μm particle 50 × 2.1 mm Acquity HSS UPLC T3 column (Waters, Milford, MA). Lipidomics acquisition performed in both pos and neg mode ionization. Pos mode lipids were normalized by Internal Standard PC 17:0; [M+H]+, Neg mode lipids were normalized by Internal Standard PC 34:0.

Metabolomics

Heart ventricle tissues were harvested from male mice at 2.5 months of age (n = 3 at each condition) and snap-frozen in liquid nitrogen. Metabolites were extracted as previously described methods [35,36]. Data were acquired in multiple reaction monitoring (MRM) using Agilent QQQ LC-MS systems. Separation of TCA and glycolysis metabolites were performed using 5 mM ammonium acetate in water as buffer pH 9.9 (A), and 100% acetonitrile as buffer (B) using Luna 3 μM NH2 column (Phenomenex, Torrance, CA) and measured 6495 triple quadrupole mass spectrometer via ESI negative mode (Agilent Technologies, Santa Clara, CA). The Gradient used is as follows: 0-20 min-80% B (Flow rate 0.2ml/min); 20-20.10 min- 80% to 2 % B; 20.10-25 min-2% B (Flow rate 0.3ml/min); 25-30 min 80% B (Flowrate 0.35ml/min); 30-35 min-80%B (Flow rate 0.4ml/min); 35-38 min 80% B (Flow rate 0.4ml/min); followed by re-equilibration at the end of the gradient to the initial starting condition 80% B at Flow rate of 0.2 ml/min. Separation and measurement of amino acids were performed using Zorbax eclipse XDB C-18, 1.8 micron, 4.6 x 100 mm column on 6495 triple quadrupole mass spectrometer via ESI Positive mode (Agilent Technologies, Santa Clara, CA). Mobile phases A and B were 0.1% formic acid in water and acetonitrile, respectively. The gradient used is as follows: 0 min-2% B; 6 min- 2% of B, 6.5 min-30 % B, 7 min-90% of B, 12 min 95% of B, 13 min 2% of B followed by re-equilibration at the end of the gradient 20 min to the initial starting condition 2% of B. Flow rate: 0.2 ml/min. Separation and measurement of CoA's and carnitines were performed using Zorbax eclipse XDB C-18, 1.8 micron, 4.6 x 100 mm column on 6495 triple quadrupole mass spectrometer via ESI Positive mode (Agilent Technologies, Santa Clara, CA). Mobile phases A and B were 0.1% formic acid in water and acetonitrile, respectively. Gradient used is as follows: 0 min-2% B; 6 min- 2% of B, 6.5 min-30 % B, 7 min- 90% of B, 12 min 95% of B,13 min 2% of B followed by re-equilibration at end of the gradient 20 min to the initial starting condition 2% of B. Flow rate: 0.2 ml/min. Separation and measurement of nucleotides were performed using Zorbax eclipse XDB C-18, 1.8 micron, 4.6 x 100 mm column on 6495 triple quadrupole mass spectrometer via ESI Positive mode (Agilent Technologies, Santa Clara, CA). Mobile phases A and B were 0.1% formic acid in water and acetonitrile, respectively. The gradient used is as follows: 0-6 min 2% B, 6-6.50 min 30% B, 7-12 min 95% B, 12-13 min 2% B, and re-equilibration till the end of the gradient 20 min. Flow rate: 0.2 ml/min). The data were normalized with internal standards, and log2 transformed on a per-sample, per-method basis. Statistical analyses were performed with either ANOVA or t-test in R Studio (R Studio Inc., Boston, MA). Differential metabolites were identified by adjusting the p-values for multiple testing at an FDR (Benjamini Hochberg method) threshold of <0.25.

Glucose tolerance test and blood metabolites measurements

For the intraperitoneal glucose tolerance test (ipGTT), mice were fasted for 6 hours (from ZT3-ZT9) and were given a 2 g/kg glucose challenge. D-(+)-Glucose (Sigma-Aldrich) was dissolved in autoclaved deionized water

at 37 °C water bath. The basal blood glucose level as well as the blood glucose levels at 15 min, 30 min, 60 min, 90 min, and 120 min after glucose injection were measured by glucometers (OneTouch Ultra 2, Lifescan). Serum insulin, FFAs, and ketone bodies were measured using Mouse Insulin ELISA Kit (Cat # 90080, Crystal Chem), Free Fatty Acid Fluorometric Assay Kit (Cat # 700310, Cayman Chemical), and β-Hydroxybutyrate LiquiColor (Cat # 2440-058, Stanbio Laboratory), respectively, following the manufacturers' instructions.

Human heart tissues and clinical data

All human hearts were obtained from the Heart Transplant Center of Fuwai Hospital, Beijing, China. The study was approved by the Ethics Committee of Fuwai Hospital. Written informed consent was obtained from patients. The 36 human heart samples were failing hearts collected from patients who underwent heart transplants between 2013 and 2018. Patients were diagnosed with idiopathic DCM according to the ESC guideline[37]. Patients with known etiology, such as hereditary conditions or valvular diseases, were excluded (**Supplemental Table S3**). Patients were not on mechanical circulatory support (LVAD). For storing the hearts in the biobank, hearts were perfused *ex vivo* using histidine-tryptophan-ketoglutarate (HTK) cardioplegia buffer before being transferred on ice for dissection. The dissected tissue samples were immediately frozen in liquid nitrogen, followed by storage at -80℃. Heart tissue samples collected in the early morning (6:00 am - 10:00 am) or late afternoon (14:00 pm - 18:00 pm) were selected. Six normal healthy hearts, once considered as donor hearts but not used for transplantation due to non-cardiac reasons, were used to set the average baseline during data analysis. The six healthy donor hearts were frozen in liquid nitrogen within 1h after clinical death (cessation of heartbeat and respiration), which was within 1d (24h) after the declaration of brain death. Organ procurement organizations coordinate the donor consent and the assessment of the potential donor organ[38]. The life-support system was withdrawn after the declaration of brain death or irreversible brain damage upon the consent of the donor's family, and the heart was then explanted after clinical death was confirmed. The surgeons involved in organ collection or transplantation did not participate in end-of-life care or the declaration of death. The collection time was defined as when tissues were frozen in liquid nitrogen. The severity of mitral regurgitation was graded using color doppler echocardiographic methods. For RT-qPCR analysis, total RNA was extracted from 60 mg/sample frozen left ventricles using Trizol. RNA yield and quality were assessed using the NanoDrop spectrophotometer (Thermo Scientific). One ug RNA was reverse transcribed into 10 ul using the PrimeScript RT Master Mix (Takara). An aliquot of each cDNA sample from normal donor hearts was pooled to generate a standard stock. Serial dilutions of the standard stock were performed to generate standard curves for quantification for each plate with the SYBR Green master mix (Thermo Fisher) on the ViiA 7 Real-Time PCR System (Thermo Fisher). The Rev-erbα/Bmal1 ratios were calculated for all heart samples. The average of the six healthy heart samples (3 in the morning, 3 in the afternoon) was used to normalize the samples from DCM patients. The resultant relative Rev-erbα/Bmal1 ratio was converted to log the scale and was used to assign groups based on the sample collection time. All available preoperative clinical data were used for data analysis.

Statistics

Littermates were used as control mice for all experiments without randomization. The sample size for each group was indicated in the figures, figure legends, or the methods section above. No statistical methods were used to pre-determine sample sizes. Instead, sample sizes were determined based on previous publications. Animals were excluded if they showed distress, infection, bleeding, or anorexia due to surgery or treatment or if they showed mis-injection at postmortem examination. Most comparisons between two groups were analyzed using a two-tailed unpaired *t*-test. Multiple groups were analyzed using two-way ANOVA with Bonferroni post hoc testing. All statistical analyses and S.E.M. calculations were based on individual mice. Normality was tested by the Shapiro-Wilk test. All tests were two-sided. Metabolomics, lipidomics, and RNA-seq were performed by experimenters who were blinded to the mouse genotype. For proteomics, the *t*-test was used for comparing two groups with $p < 0.05$ as the significant cut-off. For metabolomics, the data were normalized with internal standards and log2 transformed on a per-sample, per-method basis. Differential metabolites were identified by adjusting the p-values for multiple testing at an FDR (Benjamini Hochberg method) threshold of <0.25. For lipidomics, the missing values for lipids were imputed using the K nearest-neighbor method. The data were normalized and log2 transformed, followed by the day median normalization. The compound-by-compound *t*-test was applied to identify the top differentially regulated lipids that passed the nominal threshold $P < 0.05$, followed by the Benjamini-Hochberg procedure for FDR correction. For human clinical data, binary logistic regressions using the sigmoid function or linear regressions using affine function were performed by SPSS version 20.0 (IBM, Armonk, NY, USA), and two-sided t-tests were used for comparing two molecular

chronotypes. $P < 0.05$ was set as significant. See **Supplemental Table S6** for statistical details for each figure panel.

Data availability

RNA-seq (GSE152372) and ChIP-seq (GSE153150) data are available in GEO. Proteomics data are available in the MASSIVE repository (MSV MSV000088075) ftp://MSV000088075@massive.ucsd.edu Metabolomics and lipidomics data are available in National Metabolomics Data Repository, Project ID: PR001208, Project DOI: 10.21228/M8JX2X, Study ID: ST001915, ST001916, and ST001917. The data that support the findings of this study are available from the corresponding author upon reasonable request.

Supplemental Figures

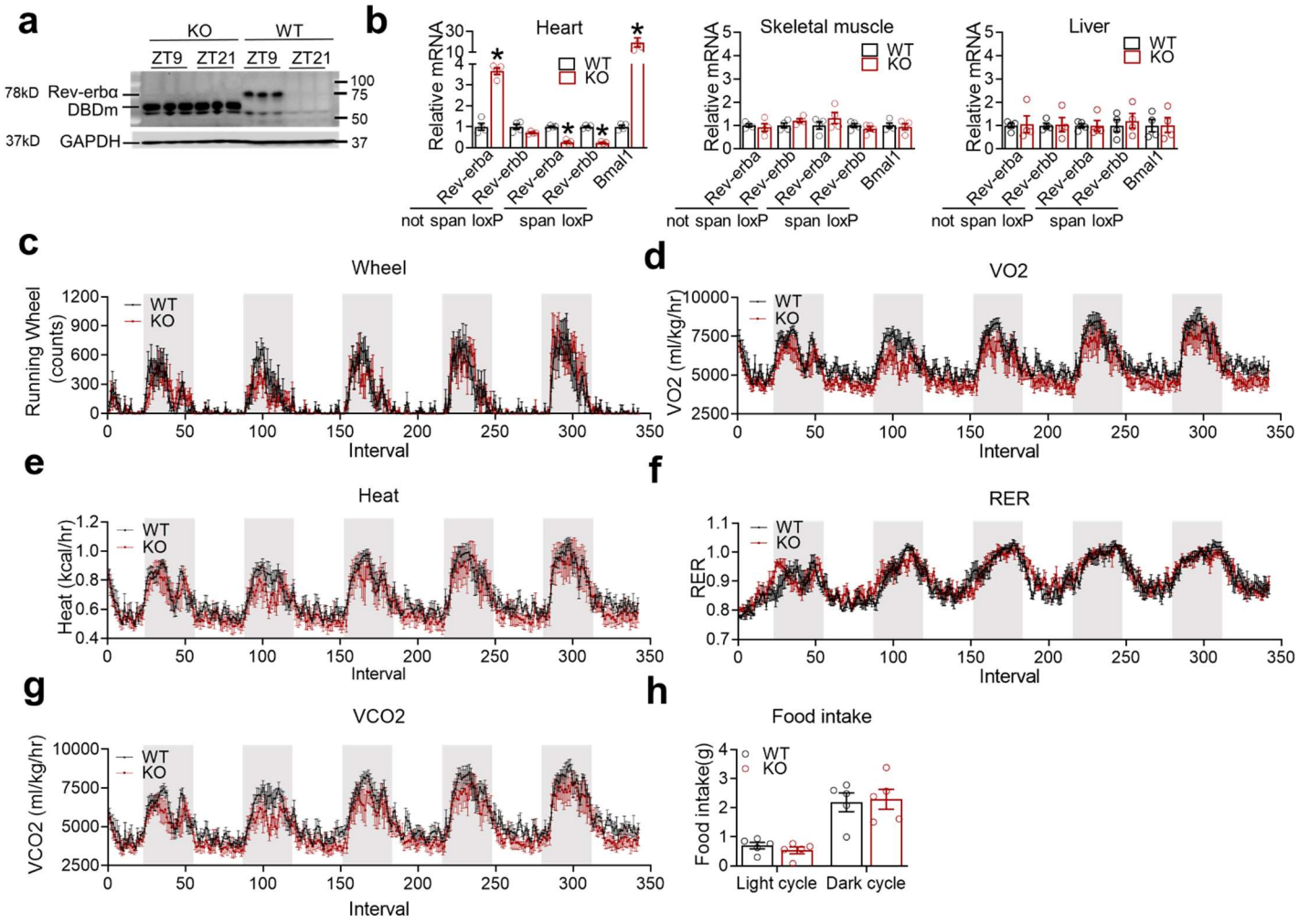

Supplemental Figure S1. Cardiomyocyte-specific ablation of Rev-erb does not affect behavioral rhythm. **(a)** Western blot analysis of Rev-erbα in the WT and KO heart in male mice at 2.5 months, n = 3 mice. **(b)** RT-qPCR analysis of the heart, quadriceps muscle, and liver in WT and KO male mice at 2.5 months using primer pairs that either span or not span the floxed exons in Rev-erbα and Rev-erbβ, n = 4 mice. **(c)** Voluntary wheel-running activities under normal light-dark cycles, n = 5 mice. **(d)** Oxygen consumption measured by indirect calorimetry, n = 5 mice. **(e)** Energy expenditure, n = 5 mice. **(f)** Respiratory exchange ratio (RER), n = 5 mice. **(g)** Carbon dioxide production, n = 5 mice. **(h)** Food intake, n = 5 mice. The sample size is indicated in the figure or described in the legend. Each dot represents an individual mouse. Data are mean ± S.E.M. * $p < 0.05$ between groups by two-sided *t*-test.

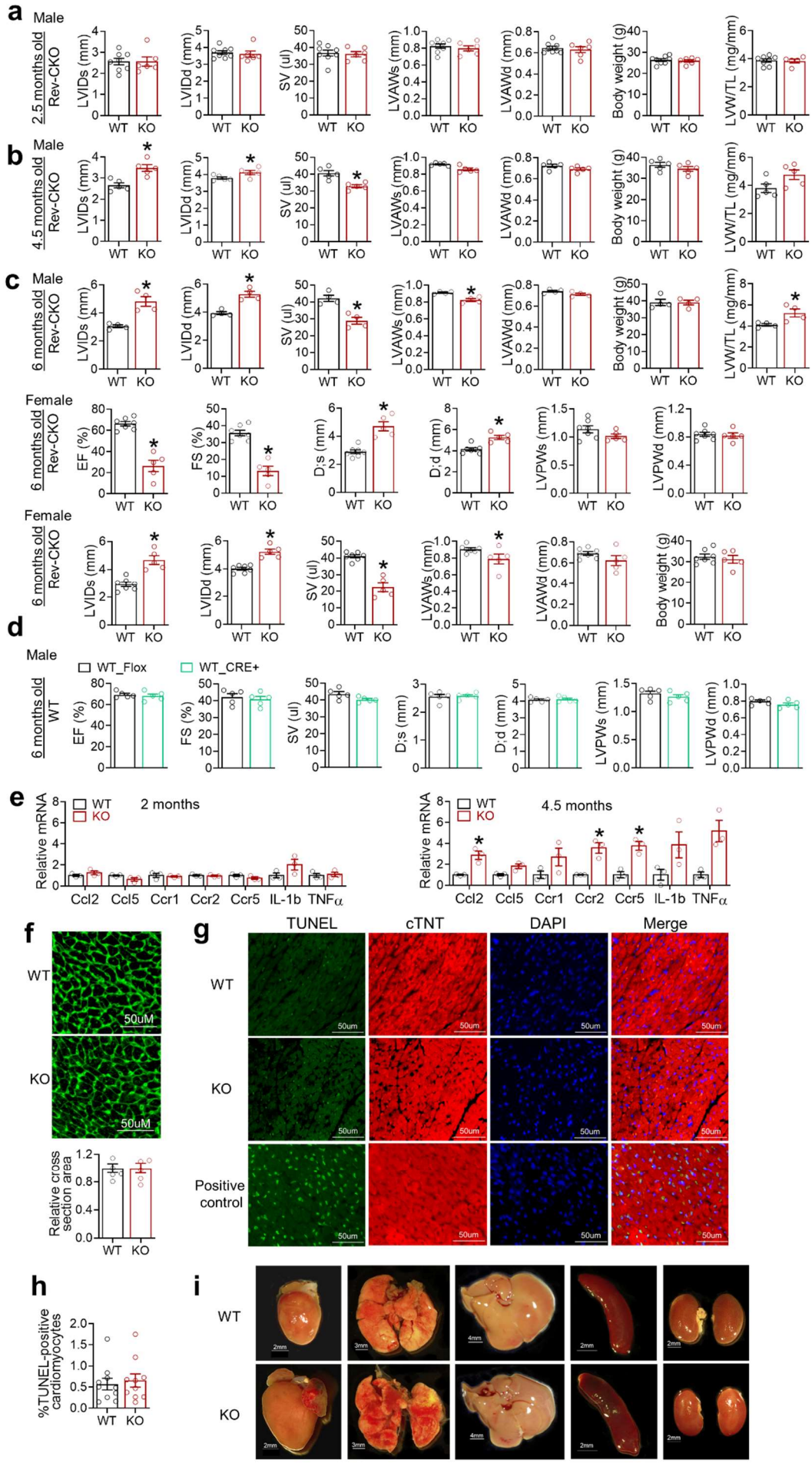
a
Male
2.5 months old Rev-CKO
b
Male
4.5 months old Rev-CKO
c
Male
6 months old Rev-CKO
Female
6 months old Rev-CKO
Female
6 months old Rev-CKO
d
Male
6 months old WT
WT_Flox
WT_CRE+
LVIDs (mm)
LVIDd (mm)
SV (ul)
LVAWs (mm)
LVAWd (mm)
Body weight (g)
LVW/TL (mg/mm)
EF (%)
FS (%)
D;s (mm)
D;d (mm)
LVPWs (mm)
LVPWd (mm)
WT
KO
e
2 months
4.5 months
Relative mRNA
Ccl2
Ccl5
Ccr1
Ccr2
Ccr5
IL-1b
TNFα
f
WT
KO
50uM
Relative cross section area
g
TUNEL
cTNT
DAPI
Merge
WT
KO
Positive control
50um
h
%TUNEL-positive cardiomyocytes
i
WT
KO
2mm
3mm
4mm

Supplemental Figure S2. Cardiomyocyte-specific ablation of Rev-erb causes progressive heart failure. **(a)** Echocardiography analysis, body weight and left ventricular weight (LVW) to tibia length (TL) ratio in male mice at 2.5 months, n = 8 mice for WT and n = 6 mice for KO. LVIDs, left ventricular internal dimension at end-systole. LVIDd, left ventricular internal dimension at end-diastole. SV, stroke volume. LVAWs, left ventricular anterior wall thickness at end-systole. LVAWd, left ventricular anterior wall thickness at end-diastole. **(b)** Echocardiography analysis, body weight and LVW/TL ratio in male mice at 4.5 months, n = 5 mice. **(c)** Echocardiography analysis, body weight and LVW/TL ratio in male or female mice at 6 months, n = 4 for male mice, n ≥ 5 for female mice. **(d)** Echocardiography analysis of WT flox/flox (WT_Flox) and WT αMHC-Cre (WT_CRE+) male mice at 6 months of age, n = 5 mice. **(e)** RT-qPCR analysis of the heart in male mice at 2 months of age and 4.5 months of age at ZT10, n = 3 mice. **(f)** Representative picture and the quantification analysis of immunostaining for wheat germ agglutinin (WGA) in male mice at 2.5 months old. Each quantification value dot represents the average value of three fields on one section. 3 mice were used for each group. **(g-h)** TUNEL assay in male mice at 2.5 months old. Sections were co-stained with cardiomyocyte marker cardiac troponin T (cTNT) and DAPI. Incubation of sections with DNase I served as the positive control. Each quantification value dot represents the average value of three fields on one section. 3 mice were used for each group. **(i)** Post-mortem pictures. The sample size is indicated in the figure. Each dot represents an individual mouse, unless otherwise stated. Data are mean ± S.E.M. * $p < 0.05$ between groups by two-sided *t*-test.

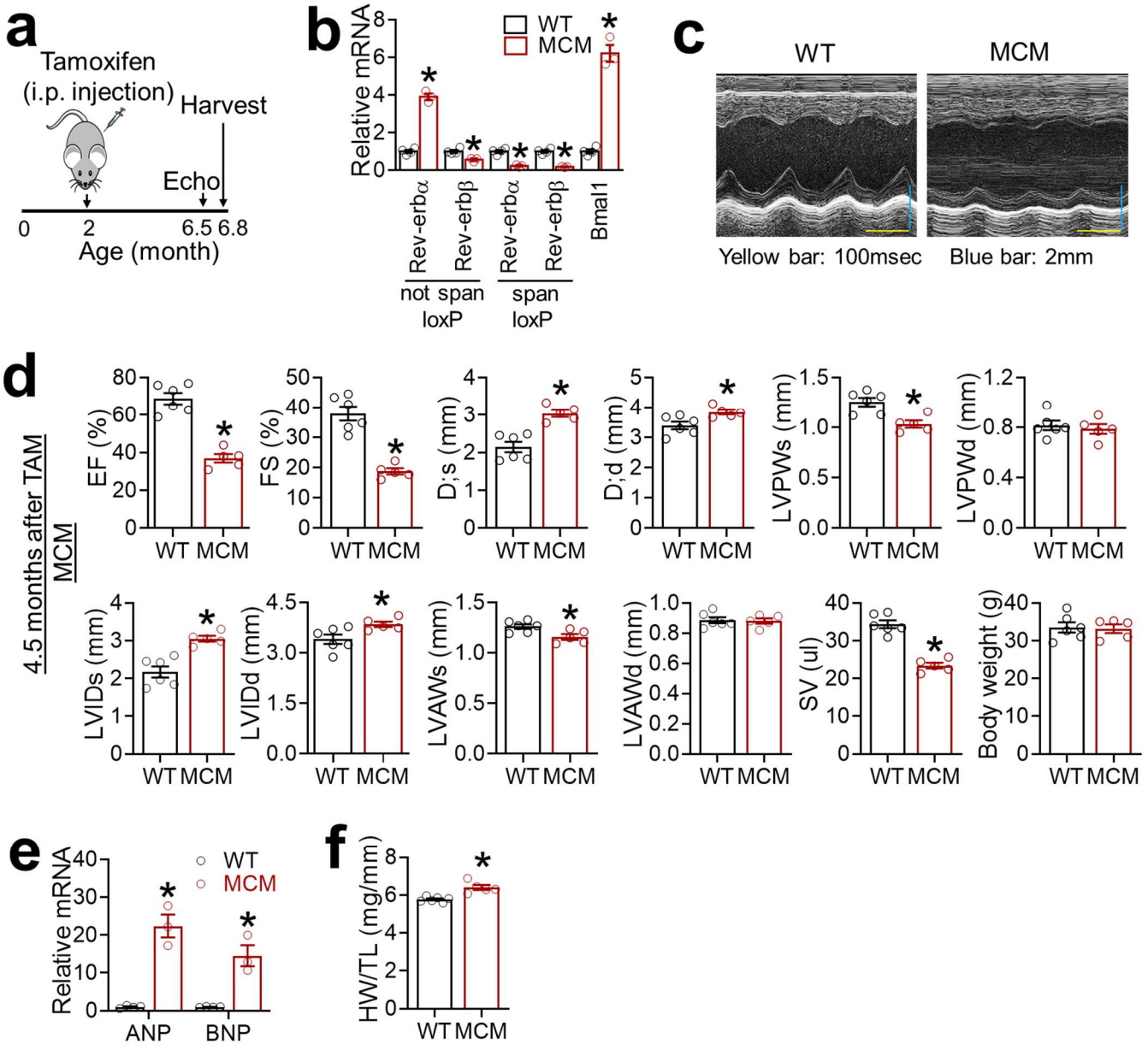

Supplemental Figure S3. Inducible ablation of Rev-erb in adult mice causes progressive heart failure. **(a)** Schematic view of tamoxifen administration and experiment timeline in MCM mice. **(b)** RT-qPCR analysis of the heart in WT and MCM male mice at 4.8 months after tamoxifen administration using primer pairs that either span or not span the floxed exons in Rev-erbα and Rev-erbβ, n = 3 mice. **(c)** Representative M mode images of echocardiography analysis in WT and MCM male mice at 4.5 months after Cre activation. **(d)** Echocardiography analysis in WT and MCM male mice at 4.5 months after tamoxifen administration, n = 6 mice for WT and n = 5 mice for MCM. **(e)** RT-qPCR analysis of the heart in WT and MCM male mice at 4.8 months after Cre activation, n = 4 mice for WT and n = 3 mice for MCM. **(f)** Heart weight (HW) to tibia length (TL) ratio in WT and MCM male mice at 4.8 months after Cre activation, n = 6 mice for WT and n = 5 mice for MCM. The sample size is indicated in the figure. Each dot represents an individual mouse. Data are mean ± S.E.M. * $p < 0.05$ between groups by two-sided *t*-test.

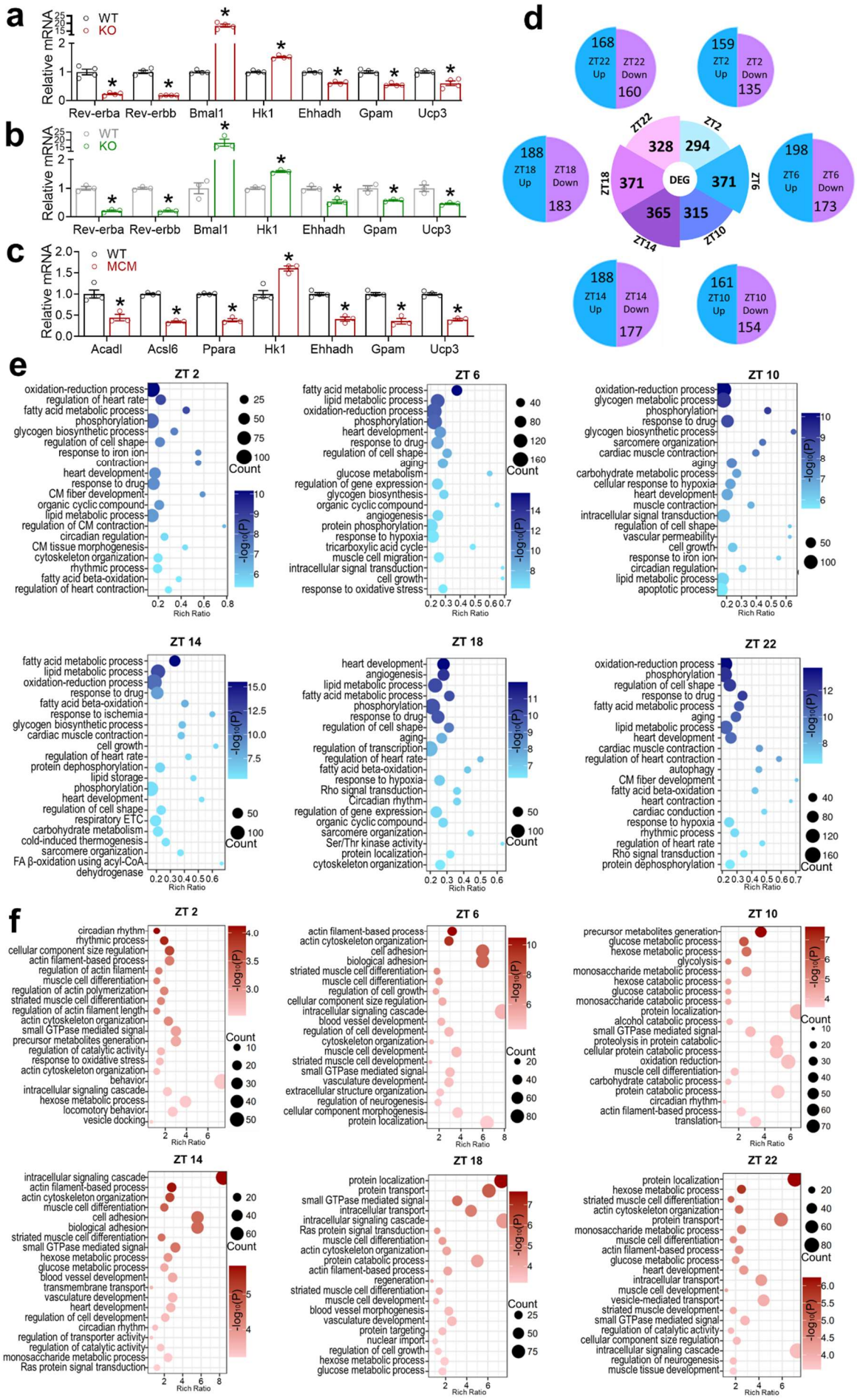
a
Relative mRNA
WT
KO
Rev-erba
Rev-erbb
Bmal1
Hk1
Ehhadh
Gpam
Ucp3
b
Relative mRNA
WT
KO
Rev-erba
Rev-erbb
Bmal1
Hk1
Ehhadh
Gpam
Ucp3
c
Relative mRNA
WT
MCM
Acadl
Acsl6
Ppara
Hk1
Ehhadh
Gpam
Ucp3
d
168
ZT22 Up
ZT22 Down
160
159
ZT2 Up
ZT2 Down
135
188
ZT18 Up
ZT18 Down
183
198
ZT6 Up
ZT6 Down
173
188
ZT14 Up
ZT14 Down
177
161
ZT10 Up
ZT10 Down
154
ZT22
ZT2
ZT18
ZT6
ZT14
ZT10
328
294
371
371
365
315
DEG
e
ZT 2
oxidation-reduction process
regulation of heart rate
fatty acid metabolic process
phosphorylation
glycogen biosynthetic process
regulation of cell shape
response to iron ion
contraction
heart development
response to drug
CM fiber development
organic cyclic compound
lipid metabolic process
regulation of CM contraction
circadian regulation
CM tissue morphogenesis
cytoskeleton organization
rhythmic process
fatty acid beta-oxidation
regulation of heart contraction
Rich Ratio
Count
-log10(P)
ZT 6
fatty acid metabolic process
lipid metabolic process
oxidation-reduction process
phosphorylation
heart development
response to drug
regulation of cell shape
aging
glucose metabolism
regulation of gene expression
glycogen biosynthesis
organic cyclic compound
angiogenesis
protein phosphorylation
response to hypoxia
tricarboxylic acid cycle
muscle cell migration
intracellular signal transduction
cell growth
response to oxidative stress
Rich Ratio
Count
-log10(P)
ZT 10
oxidation-reduction process
glycogen metabolic process
phosphorylation
response to drug
glycogen biosynthetic process
sarcomere organization
cardiac muscle contraction
aging
carbohydrate metabolic process
cellular response to hypoxia
heart development
muscle contraction
intracellular signal transduction
regulation of cell shape
vascular permeability
cell growth
response to iron ion
circadian regulation
lipid metabolic process
apoptotic process
Rich Ratio
-log10(P)
Count
ZT 14
fatty acid metabolic process
lipid metabolic process
oxidation-reduction process
response to drug
fatty acid beta-oxidation
response to ischemia
glycogen biosynthetic process
cardiac muscle contraction
cell growth
regulation of heart rate
protein dephosphorylation
lipid storage
phosphorylation
heart development
regulation of cell shape
respiratory ETC
carbohydrate metabolism
cold-induced thermogenesis
sarcomere organization
FA β-oxidation using acyl-CoA dehydrogenase
Rich Ratio
-log10(P)
Count
ZT 18
heart development
angiogenesis
lipid metabolic process
fatty acid metabolic process
phosphorylation
response to drug
regulation of cell shape
aging
regulation of transcription
regulation of heart rate
fatty acid beta-oxidation
response to hypoxia
Rho signal transduction
Circadian rhythm
regulation of gene expression
organic cyclic compound
sarcomere organization
Ser/Thr kinase activity
protein localization
cytoskeleton organization
Rich Ratio
-log10(P)
Count
ZT 22
oxidation-reduction process
phosphorylation
regulation of cell shape
response to drug
fatty acid metabolic process
aging
lipid metabolic process
heart development
cardiac muscle contraction
regulation of heart contraction
autophagy
CM fiber development
fatty acid beta-oxidation
heart contraction
cardiac conduction
response to hypoxia
rhythmic process
regulation of heart rate
Rho signal transduction
protein dephosphorylation
Rich Ratio
-log10(P)
Count
f
ZT 2
circadian rhythm
rhythmic process
cellular component size regulation
actin filament-based process
regulation of actin filament
muscle cell differentiation
regulation of actin polymerization
striated muscle cell differentiation
regulation of actin filament length
actin cytoskeleton organization
small GTPase mediated signal
precursor metabolites generation
regulation of catalytic activity
response to oxidative stress
actin cytoskeleton organization
behavior
intracellular signaling cascade
hexose metabolic process
locomotory behavior
vesicle docking
Rich Ratio
-log10(P)
Count
ZT 6
actin filament-based process
actin cytoskeleton organization
cell adhesion
biological adhesion
striated muscle cell differentiation
muscle cell differentiation
regulation of cell growth
cellular component size regulation
intracellular signaling cascade
blood vessel development
regulation of cell development
cytoskeleton organization
muscle cell development
striated muscle cell development
small GTPase mediated signal
vasculature development
extracellular structure organization
regulation of neurogenesis
cellular component morphogenesis
protein localization
Rich Ratio
-log10(P)
Count
ZT 10
precursor metabolites generation
glucose metabolic process
hexose metabolic process
glycolysis
monosaccharide metabolic process
hexose catabolic process
glucose catabolic process
monosaccharide catabolic process
protein localization
alcohol catabolic process
small GTPase mediated signal
proteolysis in protein catabolic
cellular protein catabolic process
oxidation reduction
muscle cell differentiation
carbohydrate catabolic process
protein catabolic process
circadian rhythm
actin filament-based process
translation
Rich Ratio
-log10(P)
Count
ZT 14
intracellular signaling cascade
actin filament-based process
actin cytoskeleton organization
muscle cell differentiation
cell adhesion
biological adhesion
striated muscle cell differentiation
small GTPase mediated signal
hexose metabolic process
glucose metabolic process
blood vessel development
transmembrane transport
vasculature development
heart development
regulation of cell development
circadian rhythm
regulation of transporter activity
regulation of catalytic activity
monosaccharide metabolic process
Ras protein signal transduction
Rich Ratio
-log10(P)
Count
ZT 18
protein localization
protein transport
small GTPase mediated signal
intracellular transport
intracellular signaling cascade
Ras protein signal transduction
muscle cell differentiation
actin cytoskeleton organization
protein catabolic process
actin filament-based process
regeneration
striated muscle cell differentiation
muscle cell development
blood vessel morphogenesis
vasculature development
protein targeting
nuclear import
regulation of cell growth
hexose metabolic process
glucose metabolic process
Rich Ratio
-log10(P)
Count
ZT 22
protein localization
hexose metabolic process
striated muscle cell differentiation
actin cytoskeleton organization
protein transport
monosaccharide metabolic process
muscle cell differentiation
actin filament-based process
glucose metabolic process
heart development
intracellular transport
muscle cell development
vesicle-mediated transport
striated muscle development
small GTPase mediated signal
regulation of catalytic activity
cellular component size regulation
intracellular signaling cascade
regulation of neurogenesis
muscle tissue development
Rich Ratio
-log10(P)
Count

Supplemental Figure S4. Transcriptomic analyses of Rev-erb function in the heart.
(a) RT-qPCR analysis of the snap-frozen heart tissues in WT and KO male mice at 2 months of age at Zeitgeber time ZT10, n = 4 mice. **(b)** RT-qPCR analysis of cardiomyocytes isolated from male mice at 2 months of age at ZT10, n = 3 mice. **(c)** RT-qPCR analysis of the snap-frozen heart tissues in WT and MCM male mice at 4.8 months after tamoxifen administration (6.8 months of age) at ZT10, n = 3 mice. **(d)** Differentially expressed genes (DEGs) in KO vs. WT at each ZT. DEGs cut-offs: $q < 0.05$ and $|Log_2\text{Fold-Change}| > 1$. **(e)** Top enriched biological process (BP) from GO analysis for downregulated DEGs ($q < 0.05$) at each ZT. **(f)** Top enriched biological process (BP) from GO analysis for upregulated DEGs ($q < 0.05$) at each ZT. Data are mean ± S.E.M. * $p < 0.05$ compared to the control group by two-sided *t*-test.

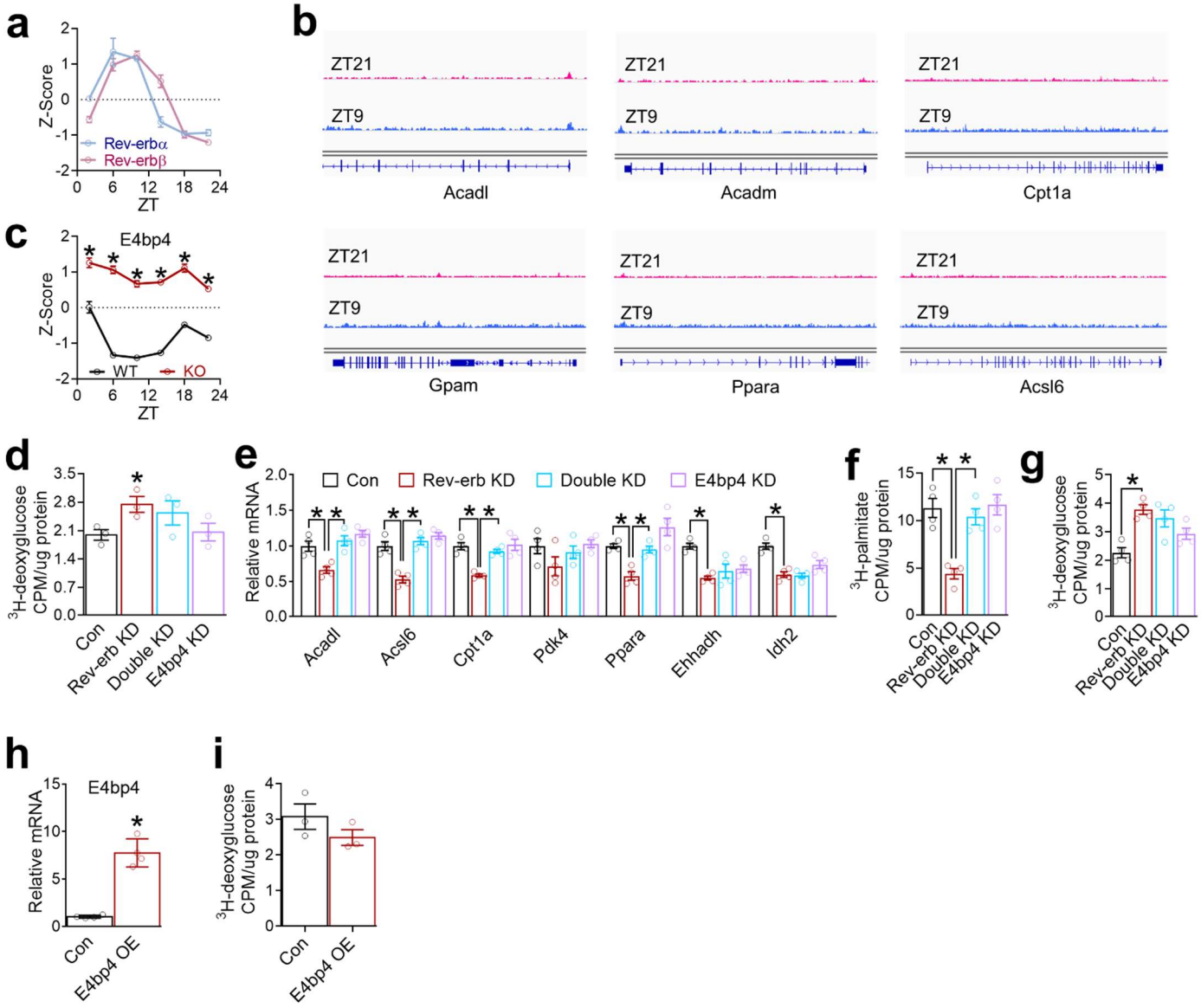

Supplemental Figure S5. E4bp4 contributes to Rev-erb-mediated cardiac transcription regulation.
(a) Relative expression levels across different ZTs for Rev-ebα, Rev-erbβ in the WT hearts based on the RNA-seq data, n = 3 mice. **(b)** Examples of Rev-erbα binding peaks at ZT21 and ZT9. **(c)** Relative expression levels of E4bp4 in the WT and KO hearts based on the RNA-seq data, n = 3 mice. * adjusted $p < 0.05$ by two-way ANOVA with Bonferroni's multiple comparisons test. **(d)** Glucose uptake in AC16 cells after knockdown of Rev-erb (Rev-erb KD) or E4bp4 (E4bp4 KD) or both (Double KD). Each dot represents an independent well of cells. **(e)** RT-qPCR analysis of primary adult mouse cardiomyocytes after siRNA-mediated knockdown of Rev-erb (Rev-erb KD) or E4bp4 (E4bp4 KD) or both (Double KD), n = 4 mice. **(f)** FAO rate in primary adult mouse cardiomyocytes, n = 4 mice. **(g)** Glucose uptake assay in primary adult mouse cardiomyocytes, n = 4 mice. **(h)** RT-qPCR analysis in AC16 cells with E4bp4 overexpression (E4bp4 OE), each dot represents an independent well of cells. **(i)** Glucose uptake assay in AC16 cells with E4bp4 overexpression (E4bp4 OE), each dot represents an independent well of cells. Data are mean ± S.E.M. * $p < 0.05$ compared to the control group by two-sided *t*-test unless otherwise stated.

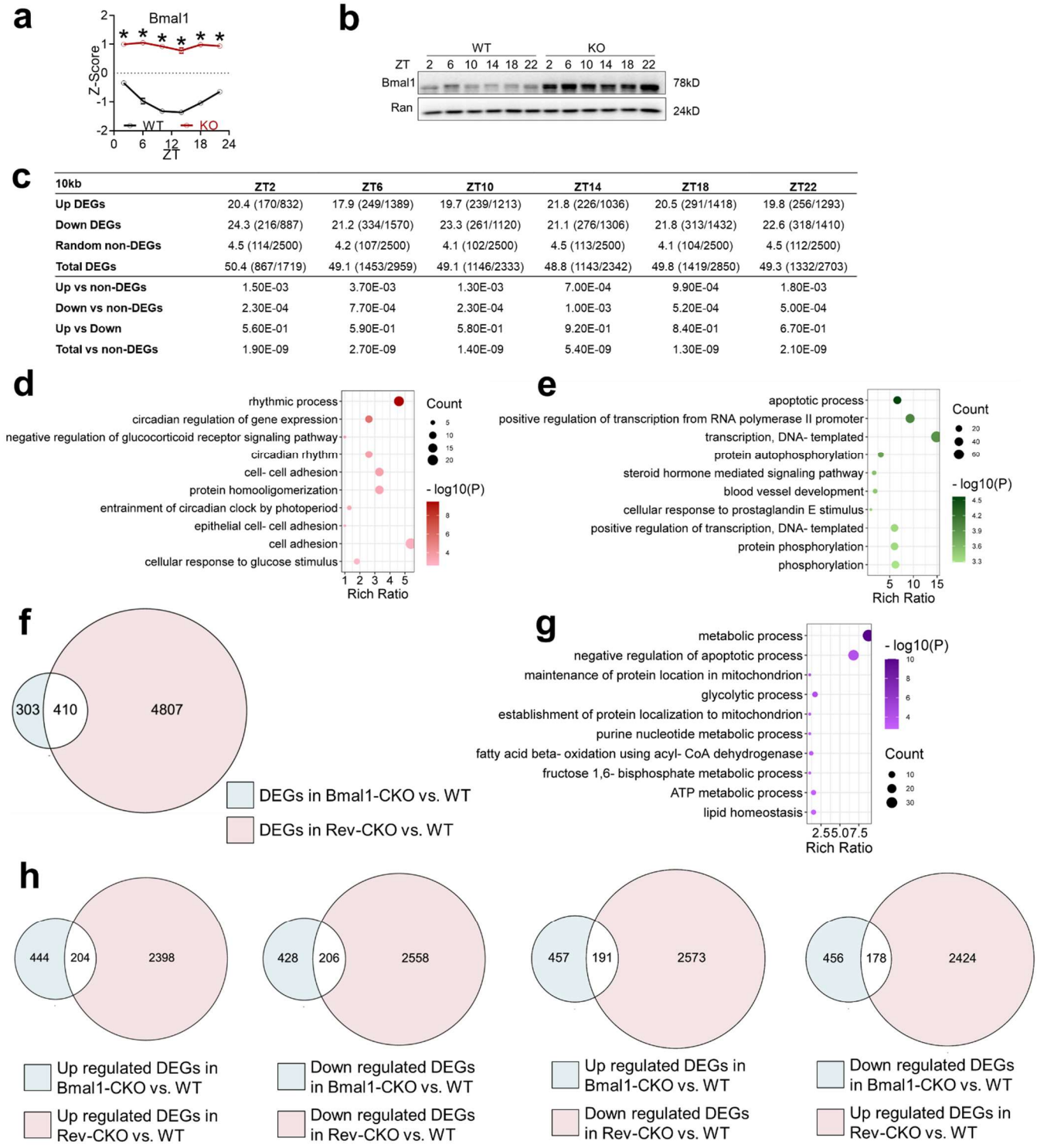

c

10kb	ZT2	ZT6	ZT10	ZT14	ZT18	ZT22
Up DEGs	20.4 (170/832)	17.9 (249/1389)	19.7 (239/1213)	21.8 (226/1036)	20.5 (291/1418)	19.8 (256/1293)
Down DEGs	24.3 (216/887)	21.2 (334/1570)	23.3 (261/1120)	21.1 (276/1306)	21.8 (313/1432)	22.6 (318/1410)
Random non-DEGs	4.5 (114/2500)	4.2 (107/2500)	4.1 (102/2500)	4.5 (113/2500)	4.1 (104/2500)	4.5 (112/2500)
Total DEGs	50.4 (867/1719)	49.1 (1453/2959)	49.1 (1146/2333)	48.8 (1143/2342)	49.8 (1419/2850)	49.3 (1332/2703)
Up vs non-DEGs	1.50E-03	3.70E-03	1.30E-03	7.00E-04	9.90E-04	1.80E-03
Down vs non-DEGs	2.30E-04	7.70E-04	2.30E-04	1.00E-03	5.20E-04	5.00E-04
Up vs Down	5.60E-01	5.90E-01	5.80E-01	9.20E-01	8.40E-01	6.70E-01
Total vs non-DEGs	1.90E-09	2.70E-09	1.40E-09	5.40E-09	1.30E-09	2.10E-09

Supplemental Figure S6. Potential role of Bmal1 in Rev-erb-mediated cardiac transcription regulation. **(a)** Relative expression levels of Bmal1 in WT and KO heart based on the RNA-seq data, n = 3 mice. * adjusted $p < 0.05$ by two-way ANOVA with Bonferroni's multiple comparisons test. **(b)** Western blot analysis of Bmal1 in WT and KO hearts. **(c)** Percentile enrichment (# of peaks / # of DEGs X 100) of Bmal1 ChIP-seq peaks (GSE110602) within 10kb of the transcription start sites (TSSs) of DEGs in Rev-CKO vs. WT mice at the indicated ZTs. P-value by Chi-square test. **(d)** Top enriched biological process (BP) from GO analysis for upregulated DEGs in Rev-CKO vs. WT mice with Bmal1 ChIP-seq peaks within 10kb of TSSs. **(e)** Top enriched biological process (BP) from GO analysis for upregulated DEGs in Rev-CKO vs. WT mice with Bmal1 ChIP-seq peaks within 10kb of TSSs. **(f)** Overlap of DEGs from Bmal1-CKO vs. WT hearts (GSE43073) and DEGs of Rev-CKO vs. WT hearts. **(g)** Top enriched biological process (BP) from GO analysis for overlapped DEGs in f. **(h)** Stratified overlap between DEGs in Bmal1-CKO and Rev-CKO hearts compared to their respective controls.

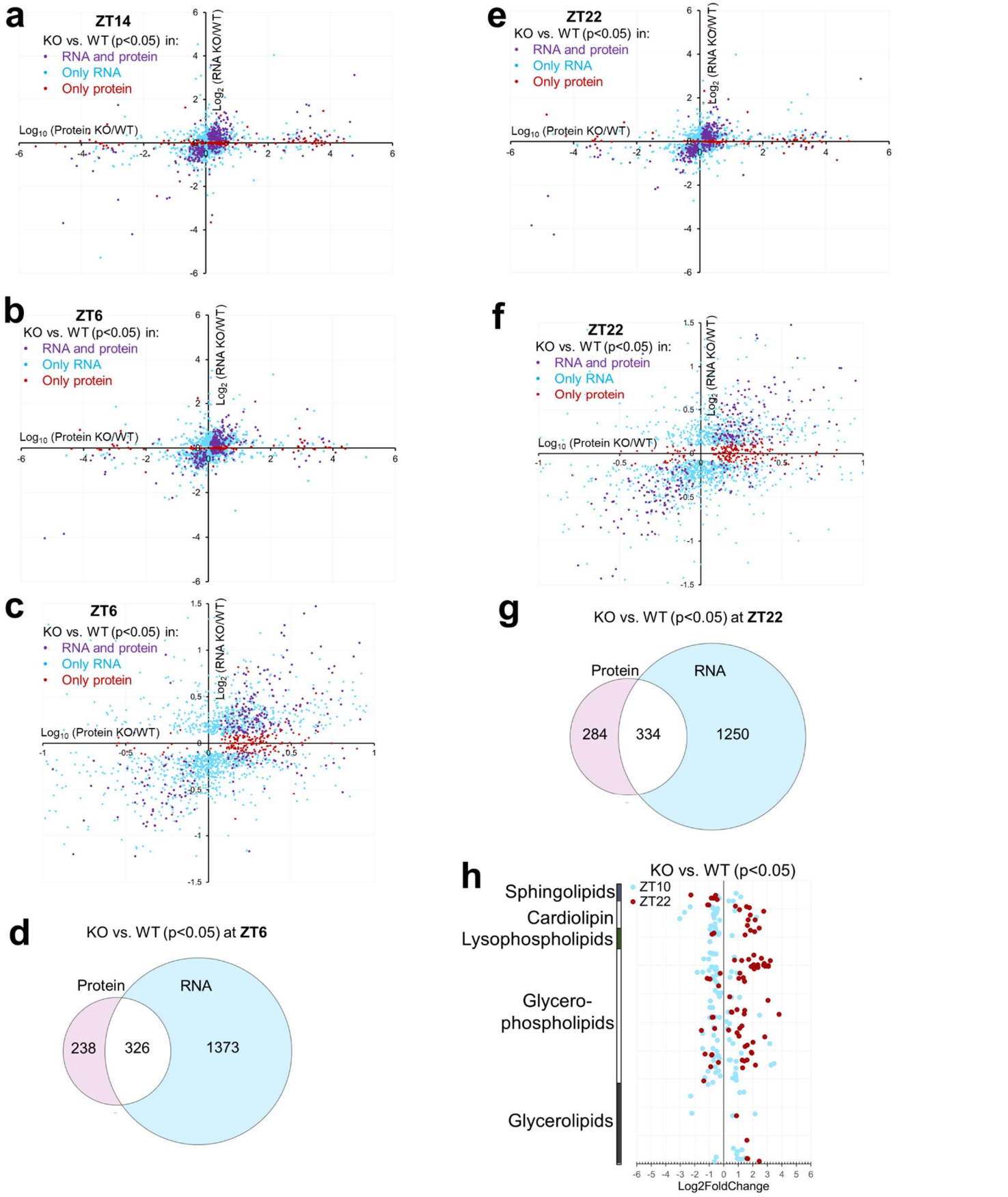

Supplemental Figure S7. Integrated transcriptomics, proteomics, and lipidomics analysis.
(a-g) Correlation and overlap of the DEGs and DEPs (KO vs. WT) at the indicated ZTs using p<0.05 as the cut-off for both RNA and protein. **(h)** Cardiac lipid species with differential levels for the indicated comparisons, n = 3 mice for each genotype at the indicated ZT.

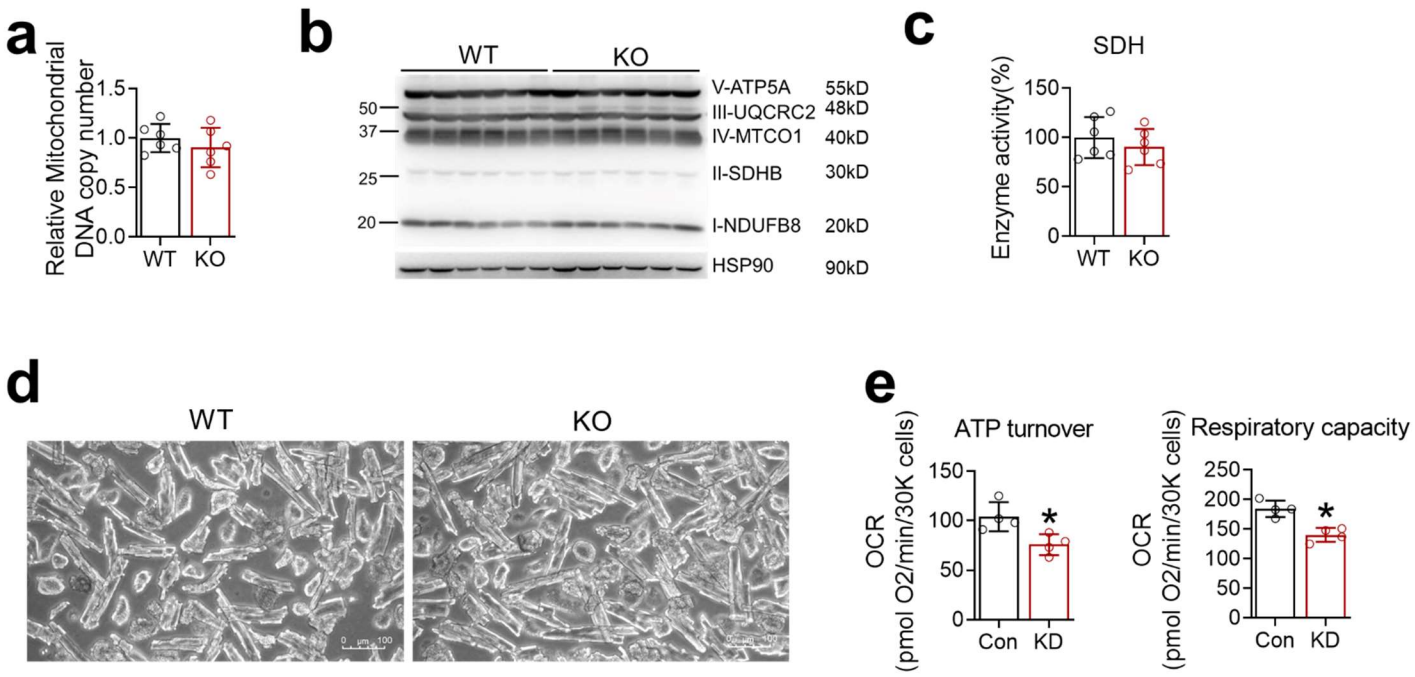

Supplemental Figure S8. Cardiac Rev-erb regulates the diurnal rhythm of myocardial metabolism.
(a) Mitochondrial DNA copy number quantification by qPCR in the WT and KO hearts, n = 6 mice. The quantification of the mitochondrial gene mtCO1 was normalized to a nuclear gene Ndufv1. **(b)** Western blot analysis of mitochondrial OXPHOS protein complexes, n = 6 mice. **(c)** Enzymatic activity of the succinate dehydrogenase (SDH) in the WT and KO hearts, n = 6 mice. **(d)** Microscopy images of primary cardiomyocytes isolated from adult mice. **(e)** Cellular respirometry analysis (Seahorse assay) of ATP turnover and respiratory capacity in AC16 cells transfected with siRNA to knockdown (KD) Rev-erb or control siRNA (Con), n = 4 wells. Data are mean ± S.E.M. * $p < 0.05$ between groups by two-sided *t*-test.

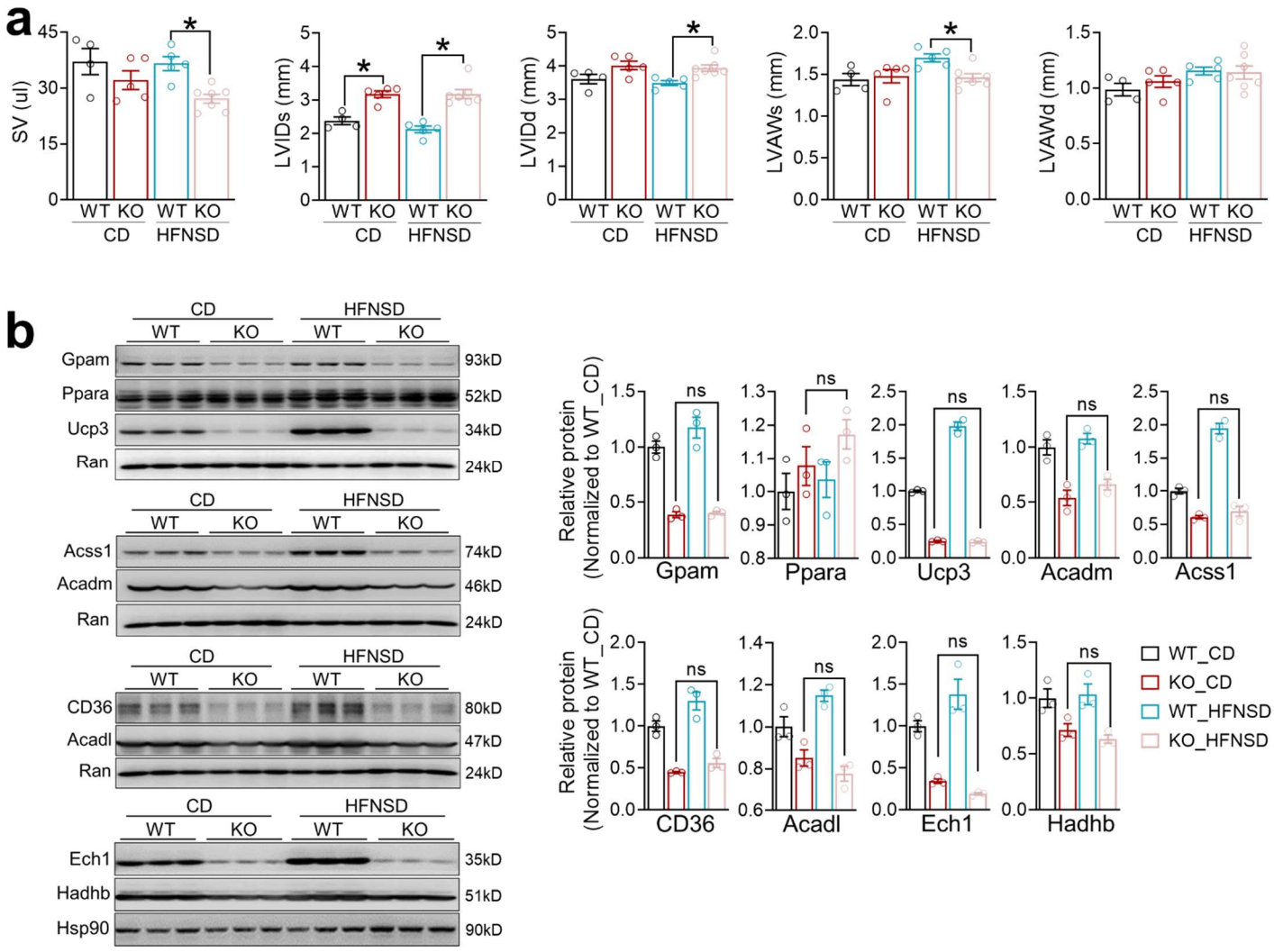

Supplemental Figure S9. HFNSD does not modulate cardiac dysfunctions in Rev-CKO mice.
(a) Echocardiography analysis on chow diet (CD) or high-fat no-sucrose diet (HFNSD) at 5 months of age in female mice, n ≥ 4 mice. **(b)** Western blot analysis of hearts in Rev-CKO and WT mice fed with CD or HFNSD, n = 3 mice. Each dot represents an individual mouse. Data are mean ± S.E.M. * $p < 0.05$ between groups by two-sided *t*-test.

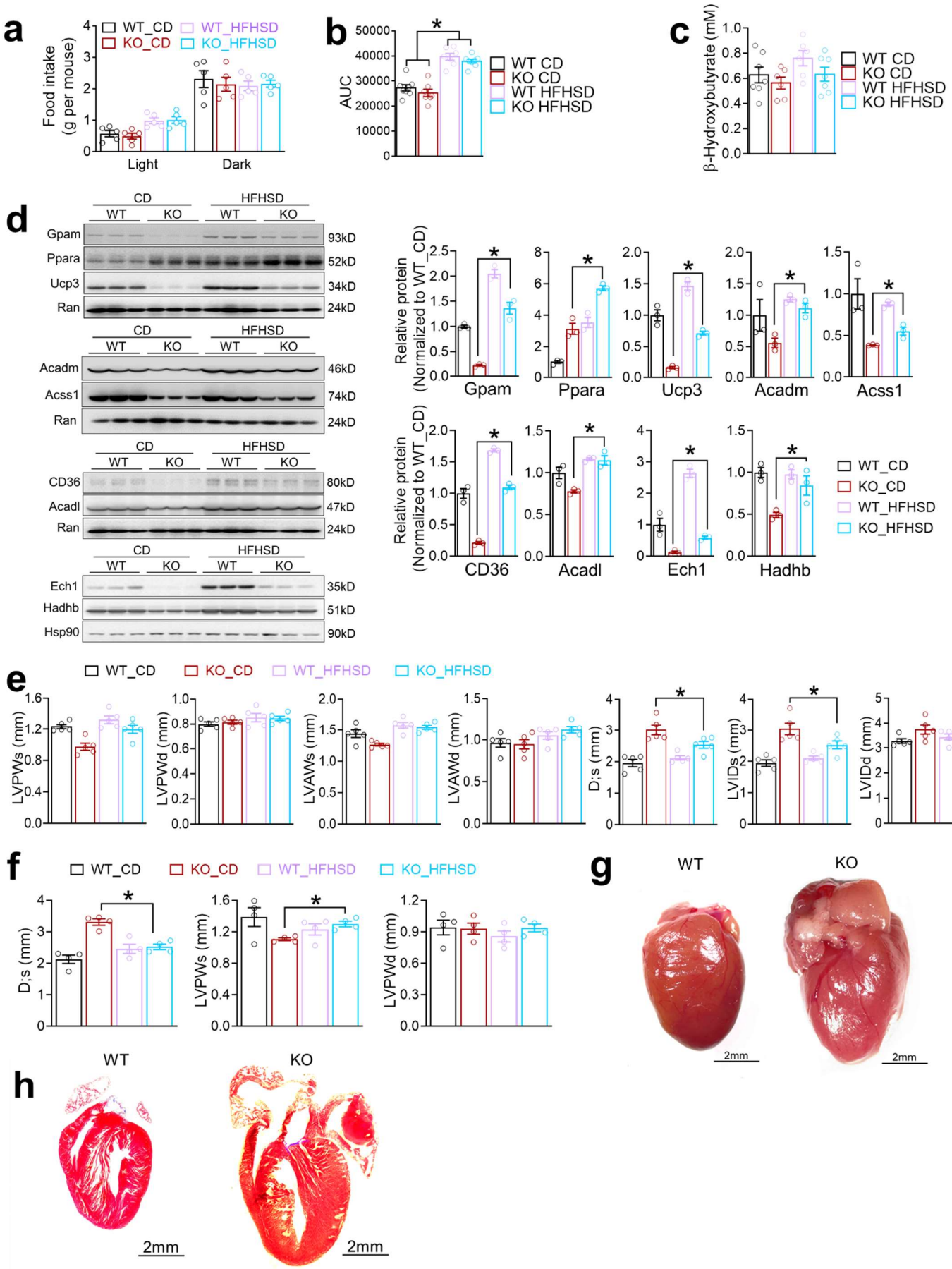
a
WT_CD
KO_CD
WT_HFHSD
KO_HFHSD
Food intake (g per mouse)
Light
Dark
b
AUC
WT CD
KO CD
WT HFHSD
KO HFHSD
c
β-Hydroxybutyrate (mM)
d
CD
HFHSD
WT
KO
Gpam
Ppara
Ucp3
Ran
Acadm
Acss1
CD36
Acadl
Ech1
Hadhb
Hsp90
93kD
52kD
34kD
24kD
46kD
74kD
80kD
47kD
35kD
51kD
90kD
Relative protein (Normalized to WT_CD)
e
LVPWs (mm)
LVPWd (mm)
LVAWs (mm)
LVAWd (mm)
D;s (mm)
LVIDs (mm)
LVIDd (mm)
f
g
WT
KO
2mm
h
2mm

Supplemental Figure S10. HFHSD modulates cardiac dysfunctions in Rev-CKO mice.
(a) Food intake for female mice fed with either CD or HFHSD, n = 5 mice. **(b)** The area under the curve (AUC) for GTT at the age of 5 months old, n ⩾ 6 mice. **(c)** Blood ketone levels in female mice at 5 months old, n ≥ 6 mice. HFHSD started at 8 weeks of age. **(d)** Western blot analysis of hearts in Rev-CKO and WT mice fed with CD or HFHSD, n = 3 mice. **(e)** Echocardiography analysis of female mice at 5 months of age on HFHSD, n = 5 mice. HFHSD started at 8 weeks of age. **(f)** Echocardiography analysis of male mice at 4.5 months of age on HFHSD, n = 4 mice. HFHSD started at 8 weeks of age. **(g-h)** Gross morphology and trichrome staining of the mouse heart harvest at 7.5 months of age on HFHSD. HFHSD started at 8 weeks of age. Each dot represents an individual mouse. Data are mean ± S.E.M. * $p < 0.05$ between groups by two-sided *t*-test.

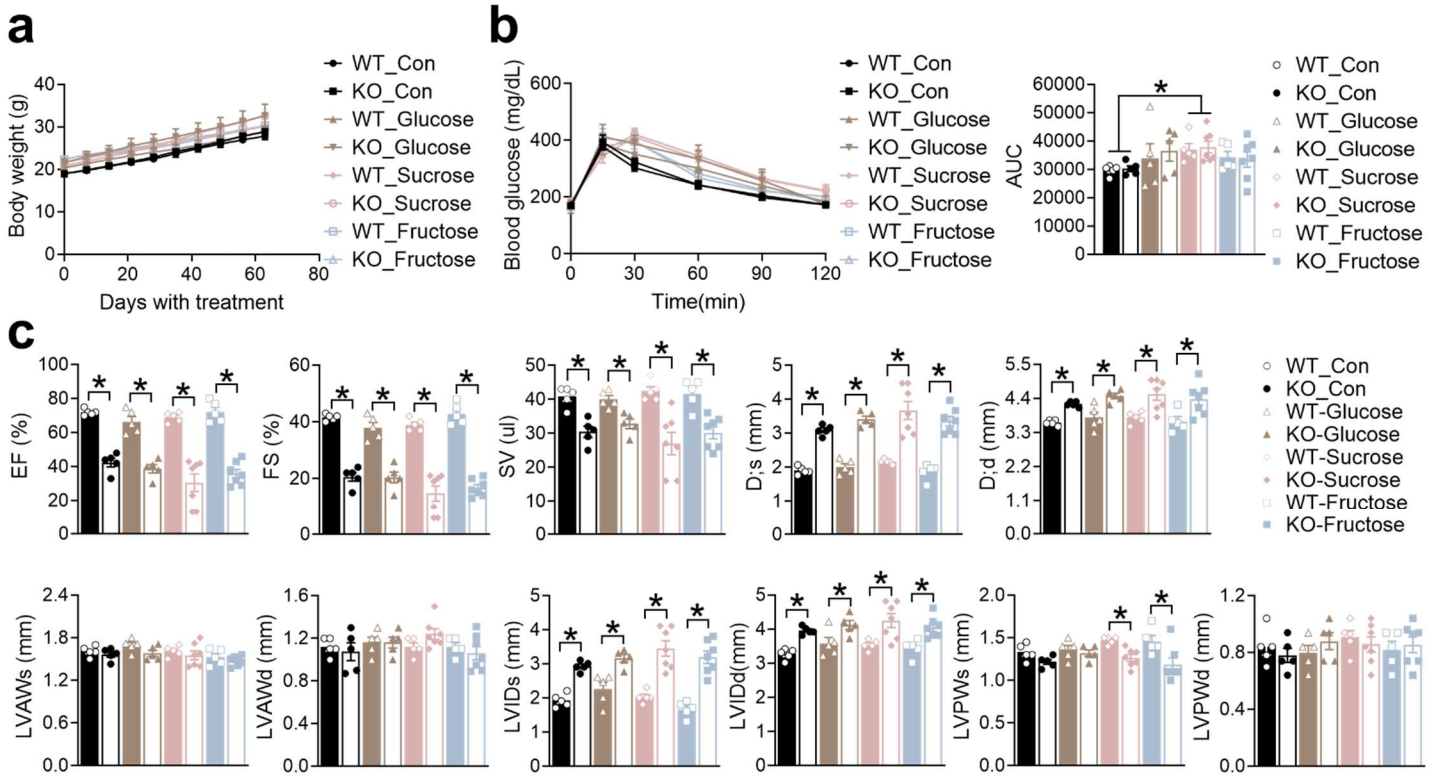

Supplemental Figure S11. High-sugar diets do not ameliorate Rev-CKO cardiac dysfunctions.
(a) Bodyweight gain in male mice drinking water containing 20% glucose, 20% sucrose, or 20% fructose, n ≥ 5 mice. The sugared water started at 8 weeks old. **(b)** GTT at 5 months of age, n ≥ 5 mice. **(c)** Echocardiography analysis of male mice at 5 months of age, n ≥ 5 mice. Data are mean ± S.E.M. * $p < 0.05$ between indicated groups by two-sided *t*-test.

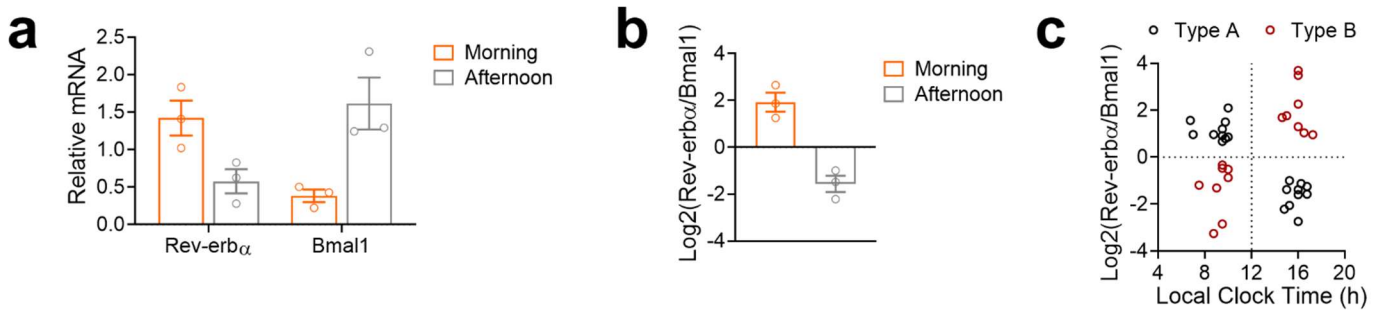

Supplemental Figure S12. **Molecular chronotypes of the cardiac molecular clock in human hearts**. **(a)** RT-qPCR analysis of normal human hearts that were once considered for transplant donors, n=3. The relative level of Rev-erbα or Bmal1 in each sample was normalized to the housekeeping gene S18 RNA and was then further normalized to the average of all 6 normal heart samples. **(b)** The ratio of Rev-erbα or Bmal1 for each sample was calculated from the above values and transformed onto the log2 scale, n=3. Data are mean ± S.E.M. **(c)** Cardiac molecular chronotype was inferred from relative gene expression levels of Rev-erbα and Bmal1 in the failing hearts of patients who received heart transplants, n = 20 patients for type A and n = 16 patients for type B.

Supplemental Tables

Supplemental Table S1. Key resources table

REAGENT or RESOURCE	SOURCE	IDENTIFIER
Chemicals, Peptides, and Recombinant Proteins		
BCA protein assay kit	Thermo Fisher Scientific	Cat # A53225
Immun-BlotÂ® PVDF Membrane, 0.22 µm	Bio-Rad Laboratories	Cat # 1620177
mouse anti-Rabbit IgG-HRP	Santa Cruz Biotechnology	Cat # sc-2357
goat anti-mouse IgG-HRP	Santa Cruz Biotechnology	Cat # sc-2005
cOmplete, EDT-free Protease Inhibitor Cocktail	Roche	Cat # 11873580001
COLLAGENASE TYPE II	Thermo Fisher Scientific	Cat # 17101015
Protease XIV (proteaseE)	Sigma	Cat # P5147
Critical Commercial Assays		
RNEASY MINI KIT	Qiagen	Cat # 74106
High-Capacity cDNA Reverse Transcription Kit	Thermo Fisher Scientific	Cat # 4368814
SYBR™ Select Master Mix	Thermo Fisher Scientific	Cat # 4472919
Isotope Tracer and Scintillation Liquid		
Deoxy-D-glucose, 2-[3H(N)]-, 250µCi (9.25MBq)	Perkinelmer	Cat # NET328250UC
Palmitic Acid, [9,10-3H(N)]-, 1mCi (185MBq)	Perkinelmer	Cat # NET043005MC
Glucose, D-[14C(U)], 250µCi (9.25MBq)	Perkinelmer	Cat # NEC042X250UC
Scintillation Liquid (Ultima Gold)	Perkinelmer	Cat # 6013326

Supplemental Table S2. Diet composition.

		HFNSD (D08060104)		HFHSD (D12492)		CD (3002906/5V5R)	
	Total Protein	26 gm%	20 kcal%	26 gm%	20 kcal%	21 gm%	23 kcal%
	Total Carbohydrate	26 gm%	20 kcal%	26 gm%	20 kcal%	56 gm%	62 kcal%
	Total Fat	35 gm%	60 kcal%	35 gm%	60 kcal%	13.5 gm%	15 kcal%
	Total Calorie	5.24 kcal/gm		5.24 kcal/gm		3.43 kcal/gm	
Ingredient		**gm**	**kcal**	**gm**	**kcal**		
Protein	Casein, Lactic	200	800	200	800		
	L-Cystine	3	12	3	12		
Carbohydrate	Corn Starch	68.8	275	0	0		
	Maltodextrin 10	125	500	125	500		
	Sucrose	0	0	68.8	275		
	Cellulose, BW200	50	0	50	0		
Fat	Soybean Oil	25	225	25	225		
	Lard	245	2205	245	2205		
Other	Mineral Mix S10026	10	0	10	0		
	DiCalcium Phosphate	13	0	13	0		
	Calcium Carbonate	5.5	0	5.5	0		
	Potassium Citrate, 1 H2O	16.5	0	16.5	0		
	Vitamin Mix V10001	10	40	10	40		
	Choline Bitartrate	2	0	2	0		
	FD&C Yellow Dye #5	0.025	0	0	0		
	FD&C Red Dye #40	0	0	0	0		
	FD&C Blue Dye #1	0.025	0	0.05	0		
Total		773.85	4057	773.85	4057		

Supplemental Table S3. Inclusion and exclusion criteria for patient samples.

Inclusion criteria
• 20 - 60 years old
• Dilated cardiomyopathy (DCM) by pathologic diagnosis
Exclusion criteria
• Familial DCM (at least one additional family member within the third-degree relatives was diagnosed with DCM) (PMID: 10099905)
• Other known cardiovascular diseases including ischemic cardiomyopathy, congenital heart diseases, and valvular diseases
• Systemic diseases
• Diabetes or with antidiabetic treatment
• Hypertension or with antihypertensive treatment
• Atrial fibrillation or use of class III anti-arrhythmic drugs
• Infectious diseases
• Abnormal renal function with eGFR < 60 mL/min/1.73 m^2
• History of drug or alcohol abuse or currently abusing alcohol or drugs
• History of myocarditis
• History of left ventricular assist device

Supplemental Table S4. General characteristics of the patients.

	Type A	Type B	P-value
Basic information			
Sample acquisition time (6-10AM/14-18PM)	10/10	8/8	>0.999 *
Age (years)	42.10 (2.28)	46.94 (2.34)	0.151
Sex ratio (male/female)	16/4	14/2	0.672 *
Body mass index (kg/m^2)	22.09 (0.84)	23.45 (1.13)	0.332
Diagnosis to transplantation (months)	6.23 (1.01)	6.13 (0.93)	0.941
Heart rate (bpm)	84.25 (3.83)	76.00 (4.27)	0.160
Systolic blood pressure (mmHg)	96.30 (2.12)	101.63 (3.47)	0.181
Diastolic blood pressure (mmHg)	69.10 (2.34)	70.63 (3.31)	0.702
Blood parameters			
Cholesterol (mmol/L)	4.36 (0.19)	4.03 (0.30)	0.343
Triglycerides (mmol/L)	1.59 (0.19)	1.62 (0.37)	0.944
HbA1c (%)	6.19 (0.19)	6.24 (0.22)	0.840
Hemoglobin (g/L)	141.00 (5.61)	133.60 (5.69)	0.370
Creatine (umol/L)	89.00 (3.60)	101.56 (6.31)	0.078
Albumin (g/L)	43.59 (1.76)	43.89 (2.74)	0.925
NTproBNP (pg/ml)	3232.58 (696.95)	3002.96 (807.37)	0.830
Sodium (mmol/L)	140.30 (0.93)	139.35 (0.64)	0.433
Urea nitrogen (mmol/L)	8.33 (0.69)	9.02 (0.76)	0.510
Uric acid (umol/L)	576.87 (42.92)	485.04 (60.79)	0.214
AST (IU/L)	71.95 (27.93)	33.88 (10.00)	0.250
ALT (IU/L)	90.70 (48.21)	44.19 (18.28)	0.416
ALP (IU/L)	71.80 (6.24)	59.81 (4.10)	0.138
CRP (mg/L)	5.72 (1.09)	4.21 (1.03)	0.330
Preoperative medication			
ACEI/ARB (user/total)	9/20	8/16	>0.999 *
β-blocker (user/total)	17/20	10/16	0.146 *
Diuretics (user/total)	15/20	12/16	>0.999 *
Cardiac status			
Heart function classification, NYHA (III/IV)	6/14	8/8	0.307 *

HbA1c, glycosylated hemoglobin Type A1c. AST, glutamic oxaloacetic transaminase. ALT, alanine aminotransferase. ALP, Alkaline phosphatase. CRP, C-reactive protein CRP. ACEI/ARB, angiotensin converting enzyme inhibitors/ angiotensin receptor blockers. Two-sided student t-test unless otherwise indicated. * Fisher test.

Supplemental Table S5. Cardiac functions in male patients only.

	Type A	Type B	P-value	P-value regression†	P-value regression‡
Age (years)	43.25 (2.58)	47.43 (2.60)	0.266		
Body mass index (kg/m2)	22.75 (0.92)	23.33 (1.28)	0.713		
Echocardiography					
Mitral regurgitation (Mild: Moderate: Large)	6:7:2	1:3:8	0.005#	0.013	0.009&
Right atrial diameter, RAD (Normal/Enlarged)	11/4	5/8	0.125*	0.063	0.063&
Interventricular septum thickness, IVS (mm)	7.91 (0.19)	9.45 (0.37)	0.002	0.017	0.001
Left ventricular end diastolic diameter, LVEDD (mm)	70.86 (2.32)	81.38 (1.94)	0.002	0.016	0.004
Left atrial anteroposterior diameter, LAD (mm)	48.33 (1.68)	59.83 (3.35)	0.007	0.387	0.005
Left ventricular posterior wall thickness, LVPW (mm)	8.31 (0.26)	9.36 (0.41)	0.036	0.052	0.045
Aortic sinus anteroposterior diameter (mm)	27.75 (2.09)	31.67 (1.33)	0.127	0.112	0.138
Aortic annular diameter, AOD (mm)	20.63 (0.94)	22.78 (0.85)	0.109	0.097	0.110
Aortic valve systolic velocity (cm/s)	0.92 (0.08)	0.83 (0.07)	0.392	0.368	0.296
Aortic valve systolic pressure difference (mmHG)	3.62 (0.63)	2.93 (0.50)	0.404	0.381	0.315
Left ventricular ejection fraction, LVEF (%)	23.31 (1.16)	26.14 (2.07)	0.229	0.215	0.375
Ascending aorta diameter (mm)	26.14 (1.15)	30.58 (1.39)	0.020	0.036	0.011
Tricuspid valve diastolic pressure difference (mmHG)	1.31 (0.23)	1.71 (0.35)	0.331	0.305	0.322
Tricuspid valve diastolic velocity (cm/s)	0.55 (0.05)	0.63 (0.06)	0.310	0.285	0.315
Mitral valve diastolic velocity (cm/s)	1.18 (0.27)	1.04 (0.09)	0.620	0.625	0.598
Main pulmonary diameter (mm)	23.88 (1.19)	28.17 (1.51)	0.043	0.068	0.069
Pulmonary valve systolic velocity (cm/s)	0.67 (0.03)	0.67 (0.12)	0.980	0.972	0.994
Tricuspid valve systolic velocity (cm/s)	3.00 (0.11)	2.74 (0.24)	0.341	0.312	0.548
Mitral valve diastolic pressure difference (mmHG)	3.93 (0.70)	4.62 (0.76)	0.516	0.493	0.653
Tricuspid valve systolic pressure difference (mmHG)	36.45 (2.55)	32.33 (3.91)	0.387	0.363	0.597
Right ventricular anteroposterior diameter, RVD (mm)	26.75 (1.86)	26.91 (1.40)	0.947	0.944	0.884
Pulmonary valve systolic pressure difference (mmHG)	1.84 (0.19)	2.10 (0.78)	0.758	0.666	0.663
MRI					
Left ventricular end diastolic diameter, LVEDD (mm)	76.46 (2.00)	86.10 (2.04)	0.003	0.015	0.002
Left atrium anteroposterior diameter, LAD (mm)	43.46 (2.46)	55.90 (3.12)	0.005	0.017	0.005
Left ventricular end diastolic volume, LVEDV (ml)	258.55 (11.46)	393.70 (66.79)	0.099	0.067	0.028
Cardiac output (L/min)	4.41 (0.58)	4.95 (0.80)	0.600	0.575	0.646
Heart rate (bpm)	84.54 (5.32)	76.89 (2.32)	0.206	0.248	0.305
Left ventricular ejection fraction, LVEF (%)	14.86 (1.44)	14.16 (1.18)	0.722	0.707	0.601

P-value: # Kruskal-Wallis rank-sum test; * Fisher's exact test; two-sided student t-test for other parameters.
† P-value regression: P-value about the correlation between the molecular chronotype and the cardiac parameter in binary logistic regressions with the molecular chronotype as the dependent variable and age, BMI, and a cardiac parameter as 3 independent variables.
‡ P-value regression: P-value about the correlation between the molecular chronotype and the cardiac parameter in linear regression models (unless otherwise indicated) with a cardiac parameter as the dependent variable and age, BMI, and molecular chronotype as 3 independent variables. & Logistic regressions were performed for these parameters. For mitral regurgitation, 'Mild' and 'Moderate' were combined as a single category

Supplemental Table S6. Statistical details.

Figures	Statistical test	Comparisons	p-value
F1a 2.5 mon ECHO EF	Unpaired t test	KO vs. WT	0.7664
F1a 2.5 mon ECHO FS	Unpaired t test	KO vs. WT	0.8068
F1a 2.5 mon ECHO D;S	Unpaired t test	KO vs. WT	0.9366
F1a 2.5 mon ECHO D;d	Unpaired t test	KO vs. WT	0.5366
F1a 2.5 mon ECHO LVPWs	Unpaired t test	KO vs. WT	0.1042
F1a 2.5 mon ECHO LVPWd	Unpaired t test	KO vs. WT	0.1921
F1b 4.5mon ECHO EF	Unpaired t test	KO vs. WT	<0.0001
F1b 4.5mon ECHO FS	Unpaired t test	KO vs. WT	<0.0001
F1b 4.5mon ECHO D;s	Unpaired t test	KO vs. WT	0.0002
F1b 4.5mon ECHO D;d	Unpaired t test	KO vs. WT	0.0042
F1b 4.5mon ECHO LVPWs	Unpaired t test	KO vs. WT	0.3843
F1b 4.5mon ECHO LVPWd	Unpaired t test	KO vs. WT	0.1766
F1c 6mon ECHO EF	Unpaired t test	KO vs. WT	<0.0001
F1c 6mon ECHO FS	Unpaired t test	KO vs. WT	0.0003
F1c 6mon ECHO D;s	Unpaired t test	KO vs. WT	0.0029
F1c 6mon ECHO D;d	Unpaired t test	KO vs. WT	0.003
F1c 6mon ECHO LVPWs	Unpaired t test	KO vs. WT	0.1426
F1c 6mon ECHO LVPWd	Unpaired t test	KO vs. WT	0.9613
F1e RT-qPCR_ANP&BNP	Unpaired t test	ANP: KO vs. WT	0.00096
F1e RT-qPCR_ANP&BNP	Unpaired t test	BNP: KO vs. WT	0.001022
F1f HW/TL	Unpaired t test	KO vs. WT	0.0241
F1i Survival	Log-rank (Mantel-Cox) test	KO vs. WT	<0.0001
F2g Acadl	Two-way ANOVA with Bonferroni's multiple comparisons test	ZT2: KO vs. WT	0.0644
		ZT6: KO vs. WT	0.0046
		ZT10: KO vs. WT	0.034
		ZT14: KO vs. WT	0.0015
		ZT18: KO vs. WT	0.0453
		ZT22: KO vs. WT	0.0081
F2g Cpt1a	Two-way ANOVA with Bonferroni's multiple comparisons test	ZT2: KO vs. WT	0.2137
		ZT6: KO vs. WT	0.1427
		ZT10: KO vs. WT	0.0156
		ZT14: KO vs. WT	0.0695
		ZT18: KO vs. WT	0.0543
		ZT22: KO vs. WT	0.1075
F2g Hadhb	Two-way ANOVA with Bonferroni's multiple comparisons test	ZT2: KO vs. WT	0.776
		ZT6: KO vs. WT	0.056
		ZT10: KO vs. WT	0.0889
		ZT14: KO vs. WT	0.0298
		ZT18: KO vs. WT	>0.9999
		ZT22: KO vs. WT	0.5269
F2g Pdk1	Two-way ANOVA with Bonferroni's multiple comparisons test	ZT2: KO vs. WT	0.359
		ZT6: KO vs. WT	0.0805
		ZT10: KO vs. WT	0.0084
		ZT14: KO vs. WT	0.0178
		ZT18: KO vs. WT	0.022
		ZT22: KO vs. WT	0.0038
F2g Acadsb	Two-way ANOVA with Bonferroni's multiple comparisons test	ZT2: KO vs. WT	0.4391
		ZT6: KO vs. WT	0.0105
		ZT10: KO vs. WT	0.2291
		ZT14: KO vs. WT	0.0186
		ZT18: KO vs. WT	0.0009
		ZT22: KO vs. WT	0.0934
F2g Acads	Two-way ANOVA with Bonferroni's multiple comparisons test	ZT2: KO vs. WT	0.512
		ZT6: KO vs. WT	0.2873
		ZT10: KO vs. WT	0.0356
		ZT14: KO vs. WT	0.0179
		ZT18: KO vs. WT	0.0399
		ZT22: KO vs. WT	0.0068
F2g Acadm	Two-way ANOVA with Bonferroni's multiple comparisons test	ZT2: KO vs. WT	0.1709
		ZT6: KO vs. WT	0.0102
		ZT10: KO vs. WT	0.0421
		ZT14: KO vs. WT	0.014
		ZT18: KO vs. WT	0.0137
		ZT22: KO vs. WT	0.0329
F2g Gpam	Two-way ANOVA with Bonferroni's multiple comparisons test	ZT2: KO vs. WT	0.5025
		ZT6: KO vs. WT	0.0819
		ZT10: KO vs. WT	0.0157
		ZT14: KO vs. WT	0.0018
		ZT18: KO vs. WT	0.0098
		ZT22: KO vs. WT	0.0091
F2g Acox1	Two-way ANOVA with Bonferroni's multiple comparisons test	ZT2: KO vs. WT	0.0001
		ZT6: KO vs. WT	0.0029
		ZT10: KO vs. WT	0.0006
		ZT14: KO vs. WT	0.0031
		ZT18: KO vs. WT	0.0004
		ZT22: KO vs. WT	0.0003
F2g Abcd3	Two-way ANOVA with Bonferroni's multiple comparisons test	ZT2: KO vs. WT	0.1112
		ZT6: KO vs. WT	0.0414

		ZT10: KO vs. WT	0.1709
		ZT14: KO vs. WT	0.0167
		ZT18: KO vs. WT	0.0162
		ZT22: KO vs. WT	0.0347
F2g Acat1	Two-way ANOVA with Bonferroni's multiple comparisons test	ZT2: KO vs. WT	0.2026
		ZT6: KO vs. WT	0.0095
		ZT10: KO vs. WT	0.211
		ZT14: KO vs. WT	0.0475
		ZT18: KO vs. WT	0.192
		ZT22: KO vs. WT	0.0028
F2g Decr1	Two-way ANOVA with Bonferroni's multiple comparisons test	ZT2: KO vs. WT	0.2012
		ZT6: KO vs. WT	0.001
		ZT10: KO vs. WT	0.0297
		ZT14: KO vs. WT	0.002
		ZT18: KO vs. WT	0.0204
		ZT22: KO vs. WT	0.0003
F2g Gck	Two-way ANOVA with Bonferroni's multiple comparisons test	ZT2: KO vs. WT	0.067
		ZT6: KO vs. WT	0.2974
		ZT10: KO vs. WT	0.0063
		ZT14: KO vs. WT	0.0966
		ZT18: KO vs. WT	0.0037
		ZT22: KO vs. WT	0.1411
F2g HK1	Two-way ANOVA with Bonferroni's multiple comparisons test	ZT2: KO vs. WT	0.082
		ZT6: KO vs. WT	0.013
		ZT10: KO vs. WT	0.0003
		ZT14: KO vs. WT	0.0007
		ZT18: KO vs. WT	0.0467
		ZT22: KO vs. WT	0.0007
F2g Eno1	Two-way ANOVA with Bonferroni's multiple comparisons test	ZT2: KO vs. WT	0.091
		ZT6: KO vs. WT	0.0574
		ZT10: KO vs. WT	>0.9999
		ZT14: KO vs. WT	0.9995
		ZT18: KO vs. WT	0.7174
		ZT22: KO vs. WT	0.001
F2g Pfkp	Two-way ANOVA with Bonferroni's multiple comparisons test	ZT2: KO vs. WT	0.0373
		ZT6: KO vs. WT	<0.0001
		ZT10: KO vs. WT	0.0109
		ZT14: KO vs. WT	0.0027
		ZT18: KO vs. WT	0.0003
		ZT22: KO vs. WT	0.0034
F3f q-PCR AC16:Rev-erb KD	Unpaired t test	Acadl: Con vs. Rev-erb KD	0.028021
		Acsl6: Con vs. Rev-erb KD	0.001026
		Cpt1a: Con vs. Rev-erb KD	0.001555
		Pdk4: Con vs. Rev-erb KD	0.000049
		Ppara: Con vs. Rev-erb KD	0.003392
		Ehhahh: Con vs. Rev-erb KD	0.002942
		Idh2: Con vs. Rev-erb KD	0.003145
F3g FAO AC16: Rev-erb KD	Unpaired t test	Con vs. KD	<0.0001
F3h Glucose uptake AC16: Rev-erb KD	Unpaired t test	Con vs. KD	0.0325
F3i q-PCR AC16_QC: Double KD	Unpaired t test	E4bp4: Con vs. Rev-erb KD	0.000098
		Bmal1: Con vs. Rev-erb KD	<0.000001
		Rev-erba: Con vs. Rev-erb KD	<0.000001
		Rev-erbb: Con vs. Rev-erb KD	<0.000001
		E4bp4: Con vs. Double KD	0.000052
		Bmal1: Con vs. Double KD	0.000014
		Rev-erba: Con vs. Double KD	<0.000001
		Rev-erbb: Con vs. Double KD	<0.000001
		E4bp4: Con vs. E4bp4 KD	<0.000001
		E4bp4: Rev-erb KD vs. Double KD	0.000008
F3j q-PCR AC16: Double KD	Unpaired t test	Acadl: Con vs. Rev-erb KD	0.007222
		Acsl6: Con vs. Rev-erb KD	0.001658
		Cpt1a: Con vs. Rev-erb KD	0.004103
		Pdk4: Con vs. Rev-erb KD	0.000423
		Ppara: Con vs. Rev-erb KD	0.001181
		Ehhahh: Con vs. Rev-erb KD	0.000452
		Idh2: Con vs. Rev-erb KD	0.002581
		Acadl: Rev-erb KD vs. Double KD	0.006675
		Acsl6: Rev-erb KD vs. Double KD	0.000392
		Cpt1a: Rev-erb KD vs. Double KD	0.014498
		Pdk4: Rev-erb KD vs. Double KD	0.001271
		Ppara: Rev-erb KD vs. Double KD	0.002549
		Ehhahh: Rev-erb KD vs. Double KD	0.551506
		Idh2: Rev-erb KD vs. Double KD	0.164852
F3k FAO AC16: Double KD	Unpaired t test	Con vs. Rev-erb KD	<0.0001
		Rev-erb KD vs. Double KD	<0.0001
F3l q-PCR AC16: E4bp4 OE	Unpaired t test	Abca1: Con vs. E4bp4 OE	0.001756
		Acsl6: Con vs. E4bp4 OE	0.001724
		Cpt1a: Con vs. E4bp4 OE	0.010756
		Stat5b: Con vs. E4bp4 OE	0.005559
		Gpam: Con vs. E4bp4 OE	0.001754
		Ppara: Con vs. E4bp4 OE	0.013577
		Pdk4: Con vs. E4bp4 OE	0.000685
		Fbp2: Con vs. E4bp4 OE	0.003434
		Pfkp: Con vs. E4bp4 OE	0.022463

		Hk1: Con vs. E4bp4 OE	0.015698
F3m FAO AC16: E4bp4 OE	Unpaired t test	Con vs. E4bp4 OE	0.0008
F3s Acadl	Two-way ANOVA with Bonferroni's multiple comparisons test	ZT6: KO vs. WT	0.0404
		ZT14: KO vs. WT	0.0434
		ZT22: KO vs. WT	0.0036
F3s Acsl6	Two-way ANOVA with Bonferroni's multiple comparisons test	ZT6: KO vs. WT	0.0171
		ZT14: KO vs. WT	0.3974
		ZT22: KO vs. WT	>0.9999
F3s Acot1	Two-way ANOVA with Bonferroni's multiple comparisons test	ZT6: KO vs. WT	0.0386
		ZT14: KO vs. WT	>0.9999
		ZT22: KO vs. WT	>0.9999
F3s Idh1	Two-way ANOVA with Bonferroni's multiple comparisons test	ZT6: KO vs. WT	0.0224
		ZT14: KO vs. WT	0.0423
		ZT22: KO vs. WT	0.0339
F3s Ech1	Two-way ANOVA with Bonferroni's multiple comparisons test	ZT6: KO vs. WT	0.0059
		ZT14: KO vs. WT	0.0387
		ZT22: KO vs. WT	0.039
F3s Ucp3	Two-way ANOVA with Bonferroni's multiple comparisons test	ZT6: KO vs. WT	0.0242
		ZT14: KO vs. WT	0.0752
		ZT22: KO vs. WT	0.2026
F3s Pgam1	Two-way ANOVA with Bonferroni's multiple comparisons test	ZT6: KO vs. WT	0.0018
		ZT14: KO vs. WT	0.0746
		ZT22: KO vs. WT	0.2799
F3s Pfkl	Two-way ANOVA with Bonferroni's multiple comparisons test	ZT6: KO vs. WT	0.0169
		ZT14: KO vs. WT	0.258
		ZT22: KO vs. WT	0.3244
F3s Pgk1	Two-way ANOVA with Bonferroni's multiple comparisons test	ZT6: KO vs. WT	0.0258
		ZT14: KO vs. WT	0.4734
		ZT22: KO vs. WT	0.3222
F3s HK1	Two-way ANOVA with Bonferroni's multiple comparisons test	ZT6: KO vs. WT	0.0344
		ZT14: KO vs. WT	0.0348
		ZT22: KO vs. WT	0.0114
F3s Pfkp	Two-way ANOVA with Bonferroni's multiple comparisons test	ZT6: KO vs. WT	0.018
		ZT14: KO vs. WT	0.0203
		ZT22: KO vs. WT	0.0285
F3s Fbp2	Two-way ANOVA with Bonferroni's multiple comparisons test	ZT6: KO vs. WT	0.573
		ZT14: KO vs. WT	0.0001
		ZT22: KO vs. WT	0.0009
F4f FAO	Unpaired t test	KO vs. WT	0.0191
F4g Glucose oxidation	Unpaired t test	KO vs. WT	0.0345
F4h glucose uptake	Unpaired t test	KO vs. WT	0.0182
F5a ECHO EF	Unpaired t test	WT_CD vs. KO_CD	0.000247
		WT_HFNSD vs. KO_HFNSD	0.000025
F5a ECHO FS	Unpaired t test	WT_CD vs. KO_CD	0.000386
		WT_HFNSD vs. KO_HFNSD	0.00002
F5a ECHO D;S	Unpaired t test	WT_CD vs. KO_CD	0.00067
		WT_HFNSD vs. KO_HFNSD	0.000211
F5a ECHO D;d	Unpaired t test	WT_CD vs. KO_CD	0.048405
		WT_HFNSD vs. KO_HFNSD	0.012955
F5a ECHO LVPWs	Unpaired t test	WT_CD vs. KO_CD	0.031501
		WT_HFNSD vs. KO_HFNSD	0.036986
F5a ECHO LVPWd	Unpaired t test	WT_CD vs. KO_CD	0.706779
		WT_HFNSD vs. KO_HFNSD	0.878401
F5b q-PCR Light cycle	Unpaired t test	Ppara: KO_CD vs. KO_HFNSD	0.626051
		Cd36: KO_CD vs. KO_HFNSD	0.821019
		Acadl: KO_CD vs. KO_HFNSD	0.367278
		Acadm: KO_CD vs. KO_HFNSD	0.059541
		Acox1: KO_CD vs. KO_HFNSD	0.320293
		Acss1: KO_CD vs. KO_HFNSD	0.687731
		Acsl6: KO_CD vs. KO_HFNSD	0.517513
		Acacb: KO_CD vs. KO_HFNSD	0.747695
		Hadhb: KO_CD vs. KO_HFNSD	0.838916
		Ech1: KO_CD vs. KO_HFNSD	0.508068
		Gpam: KO_CD vs. KO_HFNSD	0.176435
		Abca1: KO_CD vs. KO_HFNSD	0.463849
		Ucp3: KO_CD vs. KO_HFNSD	0.383126
F5b q-PCR Dark cycle	Unpaired t test	Ppara: KO_CD vs. KO_HFNSD	0.673098
		Cd36: KO_CD vs. KO_HFNSD	0.791177
		Acadl: KO_CD vs. KO_HFNSD	0.25828
		Acadm: KO_CD vs. KO_HFNSD	0.183683
		Acox1: KO_CD vs. KO_HFNSD	0.857665
		Acss1: KO_CD vs. KO_HFNSD	0.778556
		Acsl6: KO_CD vs. KO_HFNSD	0.761664
		Acacb: KO_CD vs. KO_HFNSD	0.917273
		Hadhb: KO_CD vs. KO_HFNSD	0.84348
		Ech1: KO_CD vs. KO_HFNSD	0.728381
		Gpam: KO_CD vs. KO_HFNSD	0.118155
		Abca1: KO_CD vs. KO_HFNSD	0.995273
		Ucp3: KO_CD vs. KO_HFNSD	0.971645
F5c HFNSD Food intake Calories from fat	Unpaired t test	Light: WT_CD vs. KO_CD	0.707252
		Dark: WT_CD vs. KO_CD	0.577827
		Light: WT_HFNSD vs. KO_HFNSD	0.980146
		Dark: WT_HFNSD vs. KO_HFNSD	0.328565
		Light: WT_CD vs. WT_HFNSD	0.007622

		Dark: WT_CD vs. WT_HFNSD	0.00001
		Light: KO_CD vs. KO_HFNSD	0.00368
		Dark: KO_CD vs. KO_HFNSD	<0.000001
F5d BW HFNSD	Two-way ANOVA with Bonferroni's multiple comparisons test	0 day on HFNSD: WT_HFNSD vs. WT_CD	>0.9999
		91 day on HFNSD: KO_HFNSD vs. KO_CD	0.1163
F5e GTT HFNSD	Two-way ANOVA with Bonferroni's multiple comparisons test	WT_CD vs WT_HFNSD 0 min	>0.9999
		WT_CD vs WT_HFNSD 15 min	0.0525
		WT_CD vs WT_HFNSD 30 min	0.0931
		WT_CD vs WT_HFNSD 60 min	0.3738
		WT_CD vs WT_HFNSD 90 min	>0.9999
		WT_CD vs WT_HFNSD 120 min	>0.9999
		KO_CD vs KO_HFNSD 0 min	>0.9999
		KO_CD vs KO_HFNSD 15 min	>0.9999
		KO_CD vs KO_HFNSD 30 min	0.037
		KO_CD vs KO_HFNSD 60 min	0.3396
		KO_CD vs KO_HFNSD 90 min	>0.9999
		KO_CD vs KO_HFNSD 120 min	>0.9999
F5e AUC_GTT HFNSD	Unpaired t test	KO_CD vs WT_CD	0.8729
		KO_HFNSD vs WT_HFNSD	0.3499
		WT_CD vs WT_HFNSD	0.0157
		KO_CD vs KO_HFNSD	0.04
F5f Insulin HFNSD	Unpaired t test	KO_CD vs WT_CD	0.5653
		KO_HFNSD vs WT_HFNSD	0.5095
F5g HOMA-IR HFNSD	Unpaired t test	KO_CD vs WT_CD	0.9354
		KO_HFNSD vs WT_HFNSD	0.6067
F5h b-hydroxybutyrate HFNSD	Unpaired t test	KO_CD vs WT_CD	0.9681
		KO_HFNSD vs WT_HFNSD	0.6084
F5i FFA HFNSD	Unpaired t test	KO_CD vs WT_CD	0.1052
		KO_HFNSD vs WT_HFNSD	0.2943
F6a HFHSD Food intake Calories from fat	Unpaired t test	Light: WT_CD vs. WT_HFHSD	0.000015
		Dark: WT_CD vs. WT_HFHSD	0.000005
		Light: KO_CD vs. KO_HFHSD	0.000025
		Dark: KO_CD vs. KO_HFHSD	<0.000001
F6b BW HFHSD	Unpaired t test	0 days on HFHSD: WT_CD vs. WT_HFHSD	0.782339
		82 days on HFHSD: WT_CD vs. WT_HFHSD	0.016568
		0 days on HFHSD: KO_CD vs. KO_HFHSD	0.312431
		82 days on HFHSD: KO_CD vs. KO_HFHSD	0.001429
F6c GTT HFHSD	Two-way ANOVA with Bonferroni's multiple comparisons test	WT_CD vs WT_HFNSD 0 min	>0.9999
		WT_CD vs WT_HFNSD 15 min	0.0096
		WT_CD vs WT_HFNSD 30 min	<0.0001
		WT_CD vs WT_HFNSD 60 min	0.0009
		WT_CD vs WT_HFNSD 90 min	0.18
		WT_CD vs WT_HFNSD 120 min	0.0328
		KO_CD vs KO_HFNSD 0 min	0.1718
		KO_CD vs KO_HFNSD 15 min	0.0002
		KO_CD vs KO_HFNSD 30 min	0.0002
		KO_CD vs KO_HFNSD 60 min	<0.0001
		KO_CD vs KO_HFNSD 90 min	0.0118
		KO_CD vs KO_HFNSD 120 min	0.0139
F6d Insulin HFHSD	Unpaired t test	WT_CD vs WT_HFNSD	<0.0001
		KO_CD vs KO_HFNSD	<0.0001
F6e HOMA-IR HFHSD	Unpaired t test	WT_CD vs WT_HFNSD	<0.0001
		KO_CD vs KO_HFNSD	<0.0001
F6f FFA HFHSD	Unpaired t test	WT_CD vs WT_HFNSD	<0.0001
		KO_CD vs KO_HFNSD	<0.0001
F6g HFHSD q-PCR Light cycle	Unpaired t test	Ppara: KO_CD vs. KO_HFHSD	<0.000001
		Cd36: KO_CD vs. KO_HFHSD	0.000086
		Acadl: KO_CD vs. KO_HFHSD	0.000001
		Acadm: KO_CD vs. KO_HFHSD	0.000005
		Acox1: KO_CD vs. KO_HFHSD	0.000013
		Acss1: KO_CD vs. KO_HFHSD	0.000011
		Acsl6: KO_CD vs. KO_HFHSD	0.000003
		Acacb: KO_CD vs. KO_HFHSD	0.000003
		Hadhb: KO_CD vs. KO_HFHSD	0.000101
		Ech1: KO_CD vs. KO_HFHSD	<0.000001
		Gpam: KO_CD vs. KO_HFHSD	0.000144
		Abca1: KO_CD vs. KO_HFHSD	0.000043
		Ucp3: KO_CD vs. KO_HFHSD	0.000039
F6h HFHSD q-PCR Dark cycle	Unpaired t test	Ppara: KO_CD vs. KO_HFHSD	0.465188
		Cd36: KO_CD vs. KO_HFHSD	0.94482
		Acadl: KO_CD vs. KO_HFHSD	0.257777
		Acadm: KO_CD vs. KO_HFHSD	0.6441
		Acox1: KO_CD vs. KO_HFHSD	0.995055
		Acss1: KO_CD vs. KO_HFHSD	0.720594
		Acsl6: KO_CD vs. KO_HFHSD	0.208454
		Acacb: KO_CD vs. KO_HFHSD	0.618178
		Hadhb: KO_CD vs. KO_HFHSD	0.008525
		Ech1: KO_CD vs. KO_HFHSD	0.085286
		Gpam: KO_CD vs. KO_HFHSD	0.025501
		Abca1: KO_CD vs. KO_HFHSD	0.003479
		Ucp3: KO_CD vs. KO_HFHSD	0.00203
F6k Female ECHO EF	Unpaired t test	WT_CD vs. KO_CD	<0.0001
		WT_HFHSD vs. KO_HFHSD	0.0067
		WT_CD vs. WT_HFHSD	0.5949

		KO_CD vs. KO_HFHSD	0.0004
F6k Female ECHO FS	Unpaired t test	WT_CD vs. KO_CD	<0.0001
		WT_HFHSD vs. KO_HFHSD	0.0076
		WT_CD vs. WT_HFHSD	0.5907
		KO_CD vs. KO_HFHSD	0.0004
F6k Female ECHO SV	Unpaired t test	WT_CD vs. KO_CD	<0.0001
		WT_HFHSD vs. KO_HFHSD	0.0093
		WT_CD vs. WT_HFHSD	0.6324
		KO_CD vs. KO_HFHSD	0.0005
F6k Female ECHO D;d	Unpaired t test	WT_CD vs. KO_CD	0.0014
		WT_HFHSD vs. KO_HFHSD	0.3511
		WT_CD vs. WT_HFHSD	0.1737
		KO_CD vs. KO_HFHSD	0.0409
F6m ECHO EF	Unpaired t test	WT_CD vs. KO_CD	<0.0001
		WT_HFHSD vs. KO_HFHSD	0.1256
		WT_CD vs. WT_HFHSD	0.1421
		KO_CD vs. KO_HFHSD	0.0018
F6m ECHO FS	Unpaired t test	WT_CD vs. KO_CD	0.0001
		WT_HFHSD vs. KO_HFHSD	0.3456
		WT_CD vs. WT_HFHSD	0.1158
		KO_CD vs. KO_HFHSD	0.0021
F6m ECHO SV	Unpaired t test	WT_CD vs. KO_CD	0.0075
		WT_HFHSD vs. KO_HFHSD	0.1835
		WT_CD vs. WT_HFHSD	0.3969
		KO_CD vs. KO_HFHSD	0.0409
F6m ECHO D;d	Unpaired t test	WT_CD vs. KO_CD	0.0068
		WT_HFHSD vs. KO_HFHSD	0.6241
		WT_CD vs. WT_HFHSD	0.2352
		KO_CD vs. KO_HFHSD	0.0017
F6n HW/TL	Unpaired t test	WT_CD vs. KO_CD	0.0075
		WT_HFHSD vs. KO_HFHSD	0.3175
		WT_CD vs. WT_HFHSD	0.0073
		KO_CD vs. KO_HFHSD	0.9346
F6o Survival	Gehan-Breslow-Wilcoxon test	KO_CD vs. KO_HFHSD	0.0089
F6p ECHO EF	Unpaired t test	KO_Con vs. KO_2DG(day)/Etomoxir(night)	0.012
		KO_Con vs. KO_Etomoxir(day)/2-DG(night)	0.2793
F6p ECHO FS	Unpaired t test	KO_Con vs. KO_2DG(day)/Etomoxir(night)	0.0092
		KO_Con vs. KO_Etomoxir(day)/2-DG(night)	0.2227
F6p ECHO SV	Unpaired t test	KO_Con vs. KO_2DG(day)/Etomoxir(night)	0.0008
		KO_Con vs. KO_Etomoxir(day)/2-DG(night)	0.5496
F6p HW/BW	Unpaired t test	KO_Con vs. KO_2DG(day)/Etomoxir(night)	0.0191
		KO_Con vs. KO_Etomoxir(day)/2-DG(night)	0.9708